Predictive Model for Important Ground Motion Parameters Associated with Large and Great Earthquakes

U.S. GEOLOGICAL SURVEY BULLETIN 1838

Predictive Model for Important Ground Motion Parameters Associated with Large and Great Earthquakes

By J. F. EVERNDEN and J. M. THOMSON

Presentation of data and model for prediction of seismic intensities and various other damage parameters resulting from earthquakes throughout the conterminous United States and the world

U.S. GEOLOGICAL SURVEY BULLETIN 1838

DEPARTMENT OF THE INTERIOR
DONALD PAUL HODEL, Secretary

U.S. GEOLOGICAL SURVEY
Dallas L. Peck, Director

UNITED STATES GOVERNMENT PRINTING OFFICE: 1988

For sale by the Books and Open-File Reports Section,
U.S. Geological Survey, Federal Center,
Box 25425, Denver, CO 80225

Library of Congress Cataloging in Publication Data

Evernden, J.F., 1922–
Predictive model for important ground motion parameters associated with large and great earthquakes.
(U.S. Geological Survey bulletin ; 1838)
Supt. of Docs. no.: I 19.3;1838
1. Earthquake prediction—Mathematical models. I. Thomson, Jean Marie. II. Title. III. Series.
QE75.B9 no.1838a 557.3 s 87-600483
[QE538.8] [551.2'2]

CONTENTS

FIGURES

TABLES

Predictive Model for Important Ground Motion Parameters Associated with Large and Great Earthquakes

By J.F. Evernden *and* J.M. Thomson

Abstract

This paper presents all requisite empirical data, figures, and graphs required to design a mathematical model for predicting seismic intensities and several other parameters of ground motion pertinent to risk analysis for all potentially damaging earthquakes throughout the conterminous United States. If (1) the requisite correlations of intensity and damage for building types throughout the world and (2) the pattern of k (attenuation) values throughout the world are established, the model's use can be extended worldwide.

INTRODUCTION

Many organizations, both public and private, are interested in estimating a wide variety of ground-motion-related effects associated with large and great earthquakes, such as types of ground failure, amplitudes of various types of ground motion, and expected losses to buildings of various types. Although data are adequate to build a first-generation predictive model for many parameters of interest, no such model has been generally available. This paper presents such a model. Detailed changes of interrelationships of parameters (possibly on a regional basis), as well as addition of new parameters, will probably be appropriate subsequent to testing of the model, but general use and evaluation of a model such as that proposed here seem timely. Various models purporting to perform some of the tasks of the proposed model are in use, but none has been subjected to close scrutiny and independent evaluation. Publication of this paper should encourage open discussion of these currently used but private models and hopefully lead to a new model incorporating the best features of all models now in use.

The model proposed is here applied to the conterminous United States but is immediately applicable to any part of the world by means of the additional analysis and data acquisition described in Part II of this paper.

Part I presents pertinent data relative to the parameters studied (that is, gives the data establishing the quantitative relationships within the model). Part II presents the predictive model and all pertinent figures assembled in a logical sequence for analysis. Text and figures illustrating regional predictions for some parameters requiring further discussion are included at the end.

All illustrations in this paper have been produced by computer from BASIC programs and data files and can be supplied by the authors at a scale useful for plotting data and making measurements. All programs are in HP BASIC, and all files are available on 8½-in floppy disk in either HP or IBM format. All material is available on request from the authors.

PART I: DATA AND ANALYSIS REQUIRED FOR DEVELOPMENT OF THE MODEL

Introduction

The aim of this paper is to develop a scheme, based on observations, to predict all ground motion parameters of current interest relative to large and great earthquakes. There are two possible approaches. The first is to predict each parameter independently of others, somewhat like U.S. Geological Survey Professional Paper 1360 (Ziony, 1985), in which the authors did not correlate several of the predicted parameters with others. The second is to demonstrate, if possible, close correlation of all of these parameters and thus provide the basis for a model that effectively operates by predicting a single parameter while using scaling laws for other parameters. Such a model has several attractive features, not the least of which would be the demonstration of the integrated and physically coherent character of the several ground motion parameters and the earthquake shaking process.

We now proceed to demonstrate that a model such as the one sketched in the second approach is indeed possible. As might be expected from earlier papers, we will choose seismic intensity, either Rossi-Forel intensity (RFI) or Modified Mercalli intensity (MMI), as the directly predicted quantity. Figures based on both RFI

and MMI will be included, as some intensity scales used throughout the world correlate more directly with one than with the other.

Prediction of Seismic Intensity

Several papers in the literature describe our procedures for calculating Rossi-Forel and Modified Mercalli intensities throughout the various attenuation regions of the United States (Evernden, 1975, 1983; Evernden and others, 1981; Evernden and Thomson, 1985). These papers illustrate the sensitivity of the intensity pattern to the regional attenuation characteristics and the agreement of the predictions and observations in all of the attenuation regions of the conterminous United States and eastern Asia. This scenario for predicting intensities has been elaborately described in the literature mentioned above and will not be given again. Suffice it to say that incorporation of signal persistence into the analytical model allows accurate prediction of intensities over a magnitude range from M 5.5 to at least M 8.25 (the largest historical earthquakes in the United States).

Maps of predicted intensities will be based on either saturated alluvium (J) or water table at a depth of 30 ft or greater (L). A few comments on these designations are in order. A problem in making predictions in California and elsewhere is the convention of classing all alluvial deposits as a single unit on many maps, including the 1:250,000-scale regional geologic maps of the State of California.

Digitization of such maps for use as our ground condition data base required that we treat grossly diverse materials as being of a single behavioral type. The way in which this problem was handled initially was to consider all of these materials as having the properties of very loose, medium to fine alluvium, so that the material was sensitive to the level of the water table. Thus, we used J (see table 1) as characteristic of saturated alluvium (water table at or near the surface) and L when the water table in alluvium was at a depth of 30 ft or greater. This decision was made with the realization that many of the areas classed as alluvium on the State map either were not alluvium or were of markedly compacted or very coarse alluvium, such as terraces and alluvial fans (that is, material with properties involving much greater strength than loose alluvium even when saturated). Treatment of these areas as being of L character involved assuming either a lowered water table or materials of greater coherence than loose alluvium. In the San Francisco Bay area, we long ago adopted the alluvial units established by Helley and others (1979) and the scaling of relative ground motion on these materials as suggested by the instrumental measurements of R.D. Borcherdt (written communication, 1983). We do not make corrections for depth to water table in the areas of the stronger alluvial units defined by Helley and his co-authors. Thus, whenever we have been able to improve on the State map, we have done so. In southern California, such correction for local alluvial properties has not been incorporated in our model as yet, so we continue to make a correction for depth to water table, realizing that, in most cases, there may be little sensitivity to water table because ground condition characteristics are such as to imply the lower intensities that we associate with lowered water table in loose alluvium. Thus, when Tinsley and Fumal (1985) reported little or no sensitivity to depth of water table, we believe that they were dealing with materials that never display the high intensities associated with loose alluvium. Therefore, we feel that there is no disagreement between their results and our mode of analysis.

Only in very sensitive materials is ground motion sensitive to depth to water table. In many so-called "alluvial" deposits, ground motion response is at most equivalent to our L condition. That loosely consolidated alluvium does indeed display sensitivity to depth to water table was clearly illustrated by the behavior of the materials around San Jose, Calif., in 1906 (San Francisco earthquake) and 1927 (Monterey Bay earthquake) (Evernden and others, 1981).

It was pointed out by Evernden and others (1981) and Evernden (1983) that refinements of the attenuation parameter k in increments of 0.125 (k=1.875 and 1.625 in addition to k=1.75 and 1.50) are frequently useful and logical in perfecting understanding of observed patterns of intensity. In most cases, however, 0.25 steps in the attenuation parameter are found to be adequate.

Table 1. Correlation of relative shaking units in terms of expected intensity relative to intensity on saturated alluvium

Ground-condition unit	Relative intensity compared to saturated alluvium (J)
Derived from geologic map of California:	
A	−2.5
B	−2.5
C	−2.2
D	−1.8
E	−1.7
F	−1.5
G	−1.0
H	−2.7
I	−2.7
J (saturated alluvium)	0
Alluvial units based on depth to water table:	
J[1]	0
L[2]	−1.00

[1] 0 ft < water table < 100 ft.
[2] 30 ft < water table.

Correlation of Strong Motion Parameters and Intensity

Evernden and others (1981) presented many examples of the close correlation of predicted and observed intensity patterns for earthquakes throughout the United States. Data compiled by Evernden and Thomson (1985) illustrated the correlation of intensity values and observed strong motion parameters. Further illustration of this latter correlation is presented here as the basis for establishing the requisite set of empirical relationships for our predictive model. The data that we use in our figures are restricted to those obtained at the time of the 1971 San Fernando earthquake (see Evernden and Thomson (1985) for source of intensity values used).

In this paper, we consider only those ground motion parameters of general interest—that is, maximum acceleration, root-mean-square (RMS) acceleration, maximum velocity, maximum displacement, and RMS displacement. Other parameters have been investigated, and the relevant data are available in the programs and files mentioned earlier. We consider the studied parameters in terms of the full available bandpass (0.1–25 Hz) (SM) and the four partial bandpasses used previously—0.1 to 0.5 Hz (B1), 0.5 to 3 Hz (B2), 3 to 10 Hz (B3), and 10 to 25 Hz (B4). All analysis is based on the higher of the two orthogonal components of horizontal ground motion as recorded by strong motion instruments at the time of the 1971 San Fernando earthquake.

Two types of calculations are made and illustrated in figures 1 through 5. The first type is conventional least squares, which assumes, as Evernden and Thomson (1985) did, detailed knowledge of the value of the strong motion parameter and possible error in the intensity value only. These calculations lead to the dashed lines on all figures, which are to be compared with the solid lines that follow a relation of the type:

$$\text{ground motion parameter} = A \times 2^{\text{RFI}}$$

where A is a constant. The so-called slope value on each figure is the number equivalent to the 2 in the equation above that leads to the best least-squares fit of the two sets of data (that is, log(ground motion parameter) = log (A) + intensity × log (slope)). The sigslope parameter is the standard deviation of the slope value. Simulations obtained by using random numbers of the type of model used for these calculations indicate, as expected, that the number of data points for all stations is adequate to provide an excellent estimate of the slope and standard deviation (under the assumption that all data come from the same population—that is, same intensity versus ground motion parameter relationship). If there is error in the calculated relationship because of insufficient data to fulfill the conditions of statistical theory, it is always in the direction of calculating too steep a functional relationship (too high a slope value). For figures based on data from all stations, the implied potential error is always minor.

The other relationship used for calculations (the dotted lines) is the assumption that both parameters may be in comparable error, so that the parameter minimized is the sum of the perpendicular distances of data from the best-fit relationship. The slope2 value on each figure is the slope value for this model, while the C.C. parameter is a measure of the fit of the data to the model; the better the fit, the closer C.C. is to 1.0. This second mode of analysis always leads to slope values that are flatter than those for the least-squares analysis, an expected result. In comparison studies of these two statistical models based on random numbers, the empirically imposed slope of the randomized data always lay between the dashed and dotted lines. For figures using all data, this relationship is of little relevance, as both lines are very close together. For some figures to be discussed below, marked disagreement of the dashed and dotted lines is expressive of inadequate data of too great a scatter to solidly establish the actual functional relationship for the figure. All lines (solid, dashed, and dotted) are constrained to pass through the "center of mass" of the studied population (Xbar, Ybar). As was the case in Evernden and Thomson's (1985) paper and for the reasons therein stated, the Pacoima Reservoir datum, although shown in all figures (upper margin of figures at RFI 7), is ignored in all statistical analyses.

It may be important to note that nearly all data used come from instruments in the basements or first stories of multistory buildings (all upper story observations are ignored). In other words, there are virtually no true free-field data available for the San Fernando earthquake. Whether data such as those used are critically perturbed from free-field values is uncertain. We assume that, on the average, they are not. We will assume in the following discussion that the conventional least-squares model is the more reasonable interpretation of the San Fernando earthquake strong motion data, although there does exist the possibility that the location of essentially all instruments in buildings may lead to marked failure of the assumptions of the least-squares model (that is, ground motion parameters as observed, although precise, are not accurate measures of the free-field values of such parameters and are thus not accurate in the sense supposed in the statistical model).

Most of the figures to be shown are based on all data in the basements or first stories of buildings on all types of ground, the adjustment of intensity for ground condition being as given in all previous papers except for one small change. That change is the use of a correction factor of −2.5 rather than the previous −3.0 for intensity (RFI) for granitic and metamorphic

rocks relative to saturated alluvium. Several figures will indicate −2.5 to be in distinctly better agreement with observations than −3.0 is. This correction to our previously used value of −3.0 is included in table 1 (that is, $A=-2.5$).

Figures 1 through 5 present data for several strong motion parameters versus Rossi-Forel and Modified Mercalli intensities for the full available bandwidth or for one of the four selected frequency bands. Most of the figures are based on data for all ground conditions and all sites, with the slight qualification that half of the data between intensities 6.8 and 7.2 is eliminated, there being an excessive number of data within this intensity range. Investigation of the impact of twofold decimation of data in this narrow intensity range on interpreted relationships indicated there to be no detectable effect. Further decimation did affect the calculated functional relationship between intensity and the pertinent strong motion parameter. As noted above, no upper story observations were used in any of our analyses.

As pointed out by Evernden and Thomson (1985) and as stressed repeatedly (see, for example, the paper by Evernden and others, 1981), RFI values are predictable when a twofold change in RMS acceleration is assumed to be equivalent to a one-unit change in RFI. MMI values do not so scale. Therefore, RFI values vary linearly across the tops of figures 1 through 5, while the MMI values along the bottoms of these figures show a nonuniform distribution. All calculations of functional relationships between intensity and strong motion parameters are based on RFI values. However, variations with MMI can be derived from the figures.

Maximum Acceleration versus Intensity

The several components of figure 1 present data relative to maximum acceleration and intensity. Figure 1*A* is for the full bandwidth (full bandwidth is designated by SM on all pertinent figures); figures 1*B* and 1*C* are for subsets of the data of figure 1*A*, figure 1*B* being for sites on alluvium and buildings of six stories or less and figure 1*C* being for sites on granitic or metamorphic rocks. The calculated slope and sigslope values suggest that the observations obey a slightly steeper relationship than (constant×2RFI). The difference between the 2 curve (solid line) and the least-squares (L/S) line (dashed line) leads to a difference of a factor of two in predicted maximum acceleration at RFI IX. In Part II of this paper, we will present summary plots of calculated L/S curves (fig. 14) and slope2 curves (fig. 15), which allow a user of the model to employ the set of predicted relationships that he deems most appropriate.

Figures 1*B* (alluvium) and 1*C* (hard rock) have slopes of 4.40±1.29 and 2.01±0.323, respectively, that are statistically indistinguishable at high confidence from the slope for all data (2.63±0.242). The item of most interest on each of these plots is the position of the (mean RFI, mean log(maximum acceleration)), or (Xbar, Ybar), point. The alluvium intensity values were adjusted for depth to water table, and an adjustment of −2.5 was used for the hard rock sites relative to saturated alluvium. The near identity of the Xbar, Ybar values on the two figures indicates that the intensity adjustment parameters used agree with the strong motion observations.

Figures 1*D* through 1*F* and 1*G* through 1*I* give maximum acceleration in bands 1 and 2, respectively, versus intensity; figures 1*D* and 1*G* are for all data, figures 1*E* and 1*H* are for alluvium, and figures 1*F* and 1*I* are for hard rock. As figure 1*A* does, figures 1*D* and 1*G* indicate a slope value somewhat greater than 2. The other figures indicate no statistically different slopes for all sites or for alluvium or hard rock sites and again support the case for a hard rock intensity adjustment value of −2.5.

Figures 1*J* and 1*K* give maximum acceleration in bands 3 and 4, respectively, versus intensity. The data for band 3 (3 −10 Hz) give a slope estimate indistinguishable from that for band 2. However, the data for band 4 suggest that the rate of dieoff of maximum acceleration between 10 and 25 Hz is markedly greater than that between 0.5 and 10 Hz (bands 2 and 3), the implication being that the rate of attenuation of these higher frequencies is markedly greater with distance. The alluvium and hard rock data for both bands 3 and 4 suggest a hard rock adjustment factor of −2.5.

RMS Acceleration versus Intensity

Figures 2*A* through 2*E* give RMS acceleration in the five spectral windows investigated versus intensity when data from all sites are plotted. Time windows of 10 s were used for SM and bands 2 through 4, while a time window of 20 s was used for band 1. The five slope values (2.30±0.164 for full bandwidth, 2.86±0.20 for band 1, 2.24±0.128 for band 2, 2.74±0.298 for band 3, and 5.62±1.28 for band 4) indicate slope values either indistinguishable from or slightly greater than 2 for bands 1 through 3 and, for maximum acceleration, indicate a much greater slope value for band 4. It is interesting to note that the calculated slope value for band 2, the band deemed by Evernden and Thomson (1985) to be that most closely approaching the frequency band controlling intensity values, is indistinguishable from the value of 2.0 used in the model for predicting seismic intensities (Evernden and others, 1981). As was the case for maximum acceleration, the data for alluvium and hard rock do not lead to statistically different estimates of slope and intercept (that is, they imply essentially identical Xbar, Ybar values for each population).

Maximum Velocity versus Intensity

Figures 3*A* through 3*D* give data for maximum velocity at all stations for full bandwidth and bands 1 through 3, values being so low in band 4 that they are not calculated. The slope for the full bandwidth (2.24±0.108) is as close to the intensity model value of 2 as any parameter investigated and leads to predicted values of maximum velocity at all intensities that are only very slightly different from those predicted by the 2 curve.

As with the acceleration data, the alluvium and hard rock analyses indicate that the hard rock intensity adjustment relative to saturated alluvium is best set at −2.5.

Maximum Displacement versus Intensity

Finally, there are several figures at low frequencies relative to displacement. Figures 4*A* through 4*F* show maximum displacement versus intensity. The first three (figs. 4*A*, 4*B*, 4*C*) are full bandwidth analysis of all sites, alluvium sites, and hard rock sites, respectively. The final three (figs. 4*D*, 4*E*, 4*F*) are for band 1 at the same sites. Not surprisingly, the slope and Xbar, Ybar values for full bandwidth and band 1 analysis of data from all sites are identical, the slope value being, as are most other parameters, somewhat greater than 2 (2.67±0.194 and 2.78±0.216) (figs. 4*A*, 4*D*). The identity of calculated displacements for full bandwidth and band 1 implies that there is no purpose in analyzing displacement for the higher frequency bands. The paired figures 4*B* and 4*C* and 4*E* and 4*F* again exhibit identical Xbar, Ybar values, illustrating for the last time the appropriateness of the hard rock adjustment value of −2.5 relative to saturated alluvium. It is somewhat surprising that the value of this adjustment parameter seems independent of strong motion parameter and bandwidth. Although the slope values for alluvium and hard rock may be somewhat different, this fact certainly cannot be demonstrated from the San Fernando data. The values for full bandwidth are distinctly different, but the sigslope values are so high that the slope differences are of questionable significance, particularly in light of the similarity of band 1 slope and sigslope values on figures 4*E* and 4*F*.

RMS Displacement versus Intensity

Figures 5*A* and 5*B* are for RMS displacement versus intensity for full bandwidth and band 1 data, respectively, at all sites. Again, note the essential identity of predicted parameter values as a function of intensity on both figures, both slope values and sigslope values suggesting falloff rates with intensity somewhat greater than 2. As we suggested (Evernden and Thomson, 1985), the fact that the rates of dieoff of band 1 strong motion values with decreasing intensity are greater than those for bands 2 and 3 may well be simply expressing the role of the elastic near-field terms at longer periods (the range of effective influence of these near-field terms scaling in wavelengths of the period of wave under consideration).

Summary figures of the data in figures 1 through 5 for use in the prediction scenario of this paper will be presented in Part II.

Pseudovelocity versus Intensity

Joyner and Fumal (1985) presented empirically established patterns of pseudovelocity versus earthquake magnitude and distance for California earthquakes but did not correlate their values explicitly with observed or predicted intensity values. We shall do exactly that. Our approach is to compare the pattern of predicted intensity for a particular modeled earthquake with the predicted patterns of pseudovelocity for the same modeled earthquake. We choose as the modeled earthquake a repeat of the Fort Tejon earthquake of 1857. Figure 6 gives the pattern of Rossi-Forel intensities predicted for this earthquake by the program described by Evernden and Thomson (1985) and by earlier papers. The assumed ground condition for this map is saturated alluvium (J). Joyner and Fumal said that their predictions are appropriate to "soil," a designation whose correlation with the ground conditions used in papers by Evernden and coauthors is unknown. We will let the investigation establish the correlation.

Figures 7*A* through 7*D* present the patterns of 5 percent damped pseudovelocity according to Joyner and Fumal's formulas at frequencies of 0.5, 1, 5, and 10 Hz. The units used on these figures are such that a one-unit change in value (for example, from 8 to 9 or from h to i) implies a twofold change in velocity (9 designates velocities from 80 to 113 cm/s, and j designates velocities from 113 to 160 cm/s). Thus, the plotted pseudovelocity units scale as do the predicted Rossi-Forel intensities (increase of one full RFI unit for a twofold change in predicted RMS acceleration in the intensity bandpass). Comparing figures 7*A* through 7*D* with figure 6 indicates nearly exactly matched scaling of intensity and pseudovelocity units at frequencies of 1 Hz and higher. The continued increase of pseudovelocity values near the fault for the 0.5-Hz map (fig. 7*A*), a phenomenon observed by Joyner and Fumal (1985) in the strong motion data of the Imperial Valley earthquake of 1979, is not observed in intensity data, the suggestion being that 0.5 Hz has little to do with influencing intensity values. The patterns for 1 and 5 Hz (figs. 7*B*, 7*C*) agree closely with the intensity data, even near the fault. Figure 7*E* presents the scaling of pseudovelocity with intensity on "soil" as implied by figures 7*A*, 7*B*, 7*C*, and 7*D*. Also shown on figure 7*E* is

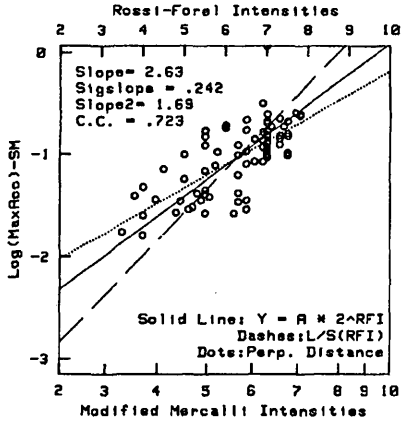

A. Full bandwidth. Data for all stations except those having Rossi-Forel intensities between 6.8 and 7.2, where decimation is by a factor of 2.

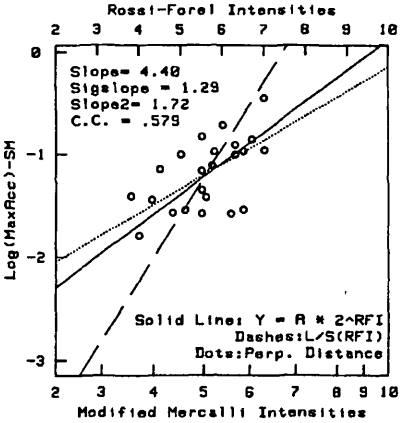

B. Full bandwidth. Data for stations on alluvium in buildings of six stories or less.

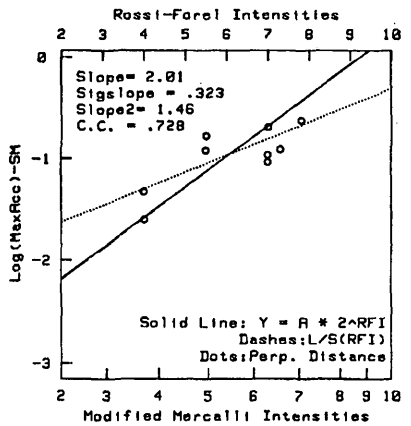

C. Full bandwidth. Data for stations on hard rock.

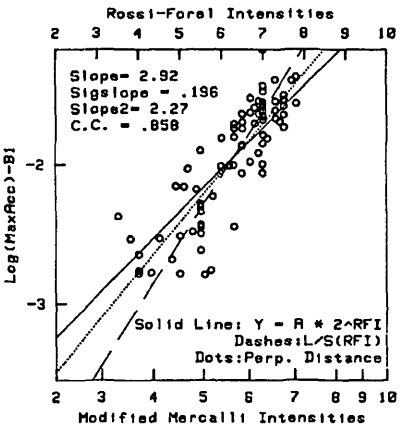

D. Band 1 (0.1–0.5 Hz). Data for all stations except those having Rossi-Forel intensities between 6.8 and 7.2, where decimation is by a factor of 2.

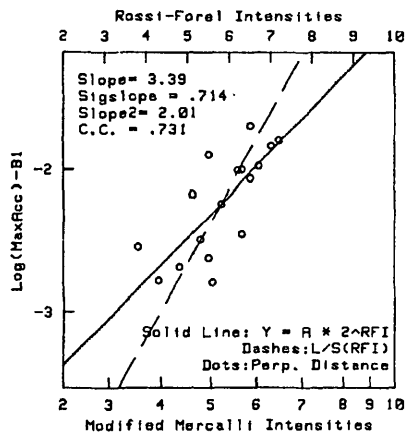

E. Band 1 (0.1–0.5 Hz). Data for stations in buildings of six stories or less on alluvium.

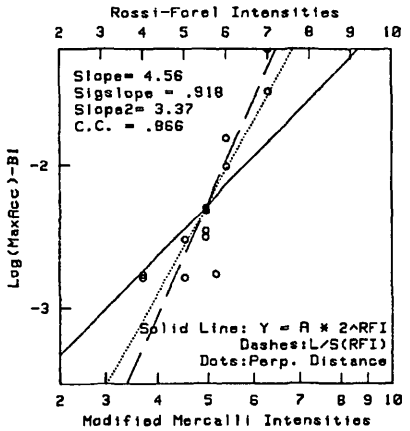

F. Band 1 (0.1–0.5 Hz). Data for stations on hard rock.

Figure 1. Maximum acceleration versus intensity for the 1971 San Fernando earthquake. Horizontal component of motion. Ground condition correction of intensities. Lines and parameters are as described in the text.

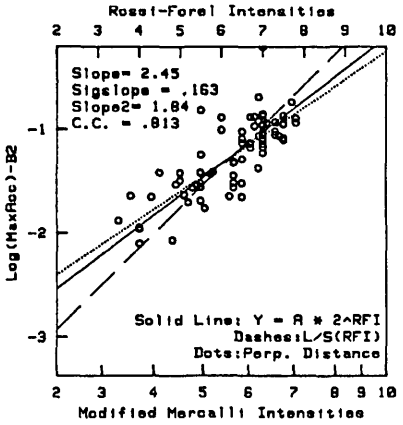

G. Band 2 (0.5–3 Hz). Data for all stations except those having Rossi-Forel intensities between 6.8 and 7.2, where decimation is by a factor of 2.

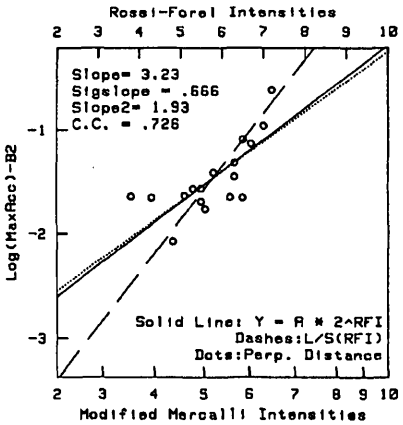

H. Band 2 (0.5–3 Hz). Data for stations on alluvium in buildings of six stories or less.

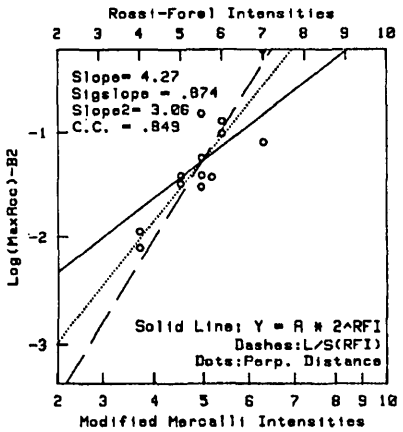

I. Band 2 (0.5–3 Hz). Data for stations on hard rock.

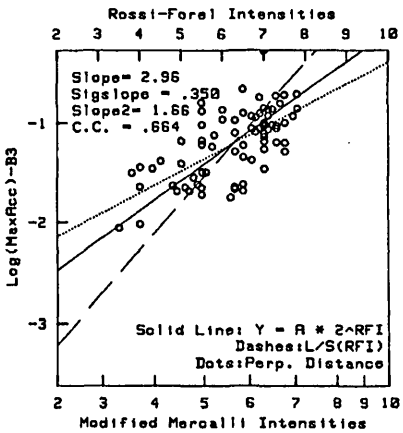

J. Band 3 (3–10 Hz). Data for all stations except those having Rossi-Forel intensities between 6.8 and 7.2, where decimation is by a factor of 2.

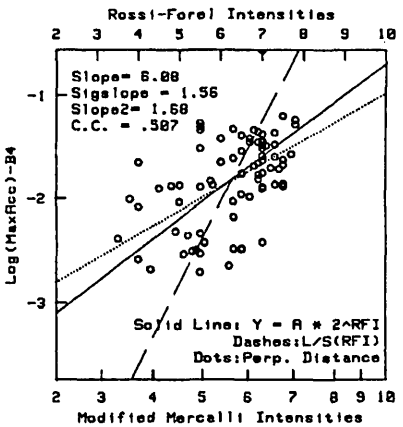

K. Band 4 (10–25 Hz). Data for all stations except those having Rossi-Forel intensities between 6.8 and 7.2, where decimation is by a factor of 2.

Figure 1. Continued.

the least-squares maximum velocity versus intensity curve for band 2 (fig. 3*C*). It can be seen that the maximum velocity curve for the bandwidth from 0.5 to 3 Hz lies between the three pseudovelocity curves for 0.5, 1, and 5 Hz and has nearly the same slope. As discussed earlier, the maximum velocity curve of figure 3*C* seems appropriate to all sites when predicted intensity is adjusted for ground condition. Therefore, in Part II, we will consider figure 7*E* (to be repeated there for convenience as fig. 16) as the basis for predicting pseudovelocity; that is, we will predict intensity (taking account of ground condition) and then read from figure 16 the implied pseudovelocity at the frequency of interest.

Correlation of Ground Failure and Intensity

Wilson and Keefer (1985, figs. 164, 174) presented empirical data as well as suggested correlations of earthquake magnitude and maximum range of observation of

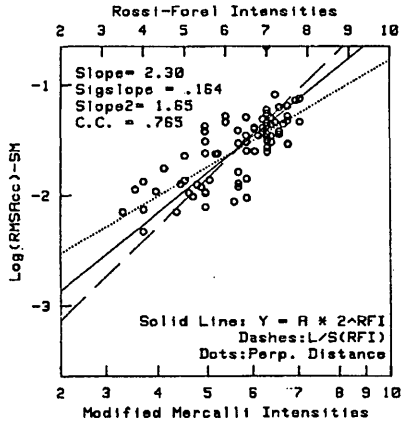

A. Full bandwidth.

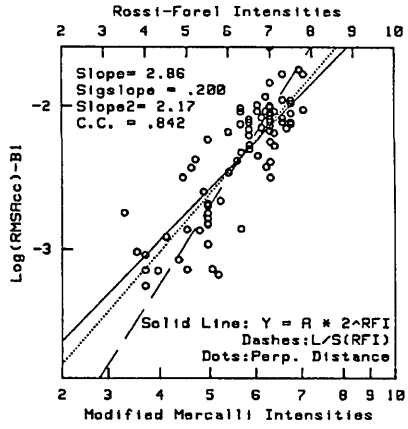

B. Band 1 (0.1–0.5 Hz).

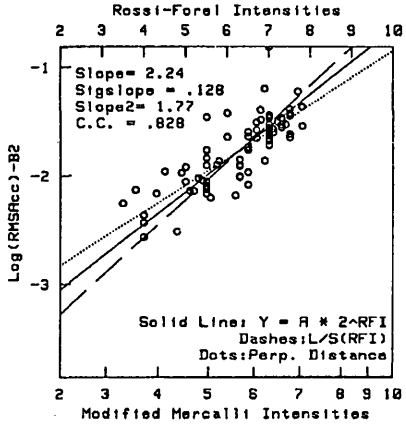

C. Band 2 (0.5–3 Hz).

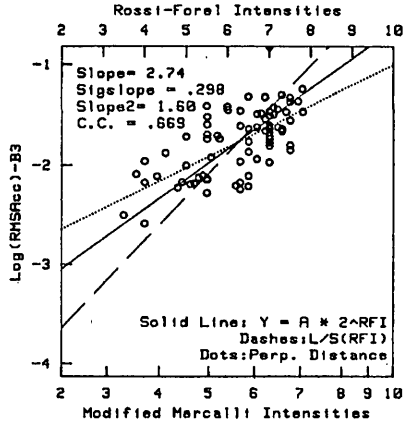

D. Band 3 (3–10 Hz).

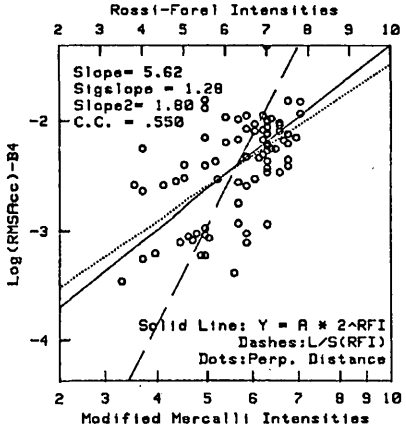

E. Band 4 (10–25 Hz).

Figure 2. RMS acceleration versus intensity for the 1971 San Fernando earthquake. Horizontal component of motion. Data for all stations except those having Rossi-Forel intensities between 6.8 and 7.2, where decimation is by a factor of 2. Ground condition correction of intensities. Lines and parameters are as described in the text.

various types of ground failure (lateral flows and spreads) (that is, liquefaction), coherent slides, and disrupted slides or falls. They combined data from all possible sources with the intent of obtaining a statistically meaningful sampling. They attempted to make the case that the magnitude-distance relationship is independent of the attenuation characteristics of the region of the earthquake, even when the data for California earthquakes clearly disagreed with any of the three relationships suggested in their figure 174*C*. The relationships given in that figure (for lateral spreads and flows) were based on Arias intensities, on Youd and Perkins' (1978) interpretation of available data for liquefaction effects of less than

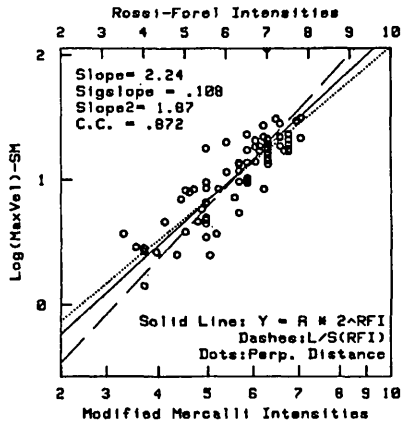

A. Full bandwidth.

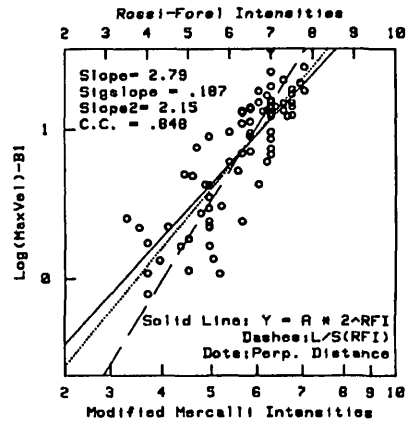

B. Band 1 (0.1–0.5 Hz).

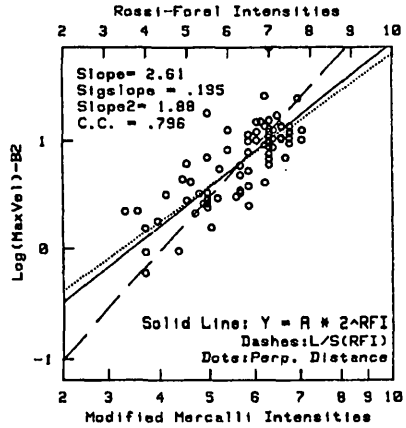

C. Band 2 (0.5–3 Hz).

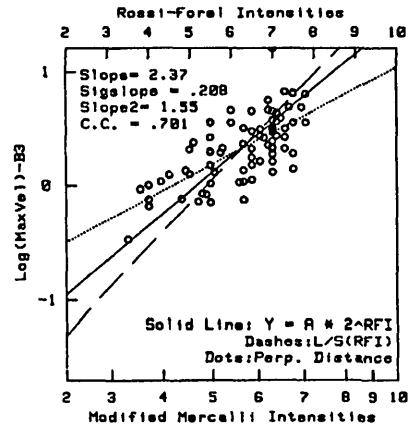

D. Band 3 (3–10 Hz).

Figure 3. Maximum velocity versus intensity for the 1971 San Fernando earthquake. Horizontal component of motion. Data for all stations except those having Rossi-Forel intensities between 6.8 and 7.2, where decimation is by a factor of 2. Ground condition correction of intensities. Lines and parameters are as described in the text.

10-cm movement, and on the maximum range to detectable liquefaction effects as interpreted by Wilson and Keefer. The curves based on Arias intensities cannot be used, as they disagree with observations at high magnitudes, the Arias curves displaying no tendency to saturate with increasing magnitude. Also, the magnitude-liquefaction-distance relationship for these curves at lower magnitudes does not agree with intensity predictions. The other two relationships shown by Wilson and Keefer were investigated relative to predicted intensities for California earthquakes. Both relationships, when investigated relative to earthquakes of varying size, showed physically uninterpretable relationships in that the implied correlation of ground motion parameter and intensity varied grossly as a function of earthquake size, extending to lower and lower intensity with increasing magnitude. Since, as we discussed above and in our earlier paper (Evernden and Thomson, 1985), predicted intensities show strong correlation with ground motion parameters as measured by strong motion seismometers, failure of interpreted ground failure parameters to agree even approximately with predicted intensities is surprising, to say the least.

When it is noted that the California data used by Wilson and Keefer disagree with their suggested empirical relationships of distance and magnitude, investigation of the California data versus predicted intensities for California earthquakes is suggested. Figures 8*A*, 8*B*, 9*A*, 9*B*, 10*A*, and 10*B* give the results of such an investigation. Figures 8*A*, 9*A*, and 10*A* give predicted Rossi-Forel

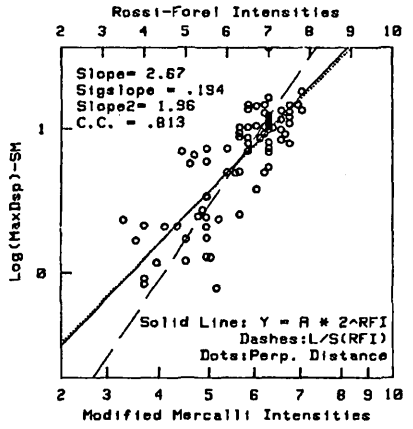

A. Full bandwidth. Data for all stations except those having Rossi-Forel intensities between 6.8 and 7.2, where decimation is by a factor of 2.

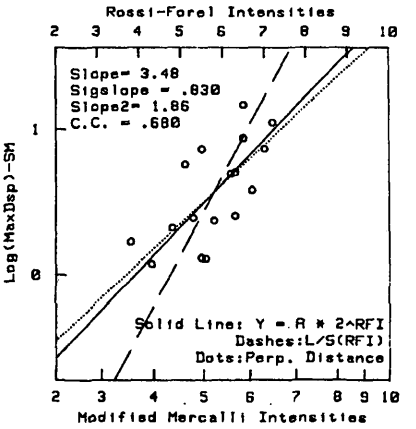

B. Full bandwidth. Data for stations in buildings of six stories or less on alluvium.

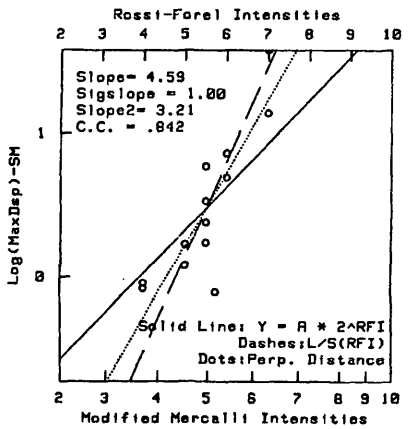

C. Full bandwidth. Data for stations on hard rock.

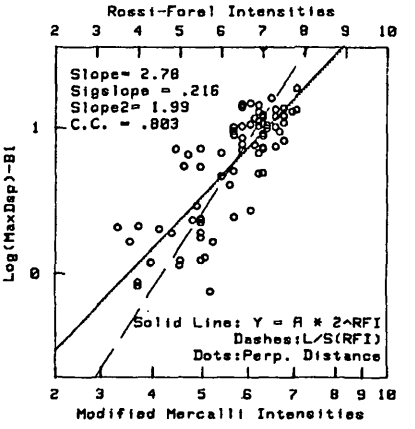

D. Band 1 (0.1–0.5 Hz). Data for all stations except those having Rossi-Forel intensities between 6.8 and 7.2, where decimation is by a factor of 2.

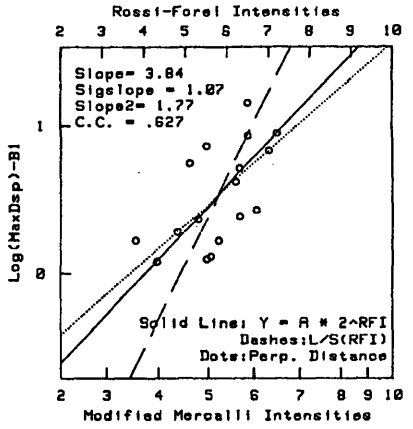

E. Band 1 (0.1–0.5 Hz). Data for stations in buildings of six stories or less on alluvium.

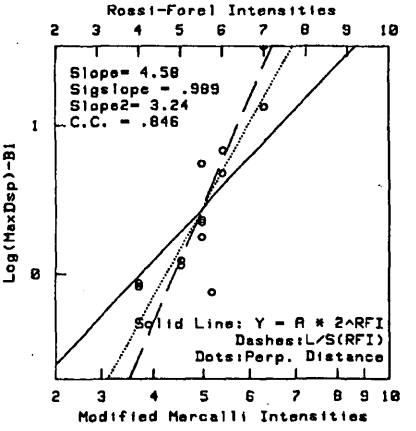

F. Band 1 (0.1–0.5 Hz). Data for stations on hard rock.

Figure 4. Maximum displacement versus intensity data for the 1971 San Fernando earthquake. Horizontal component of motion. Ground condition correction of intensities. Lines and parameters are as described in the text.

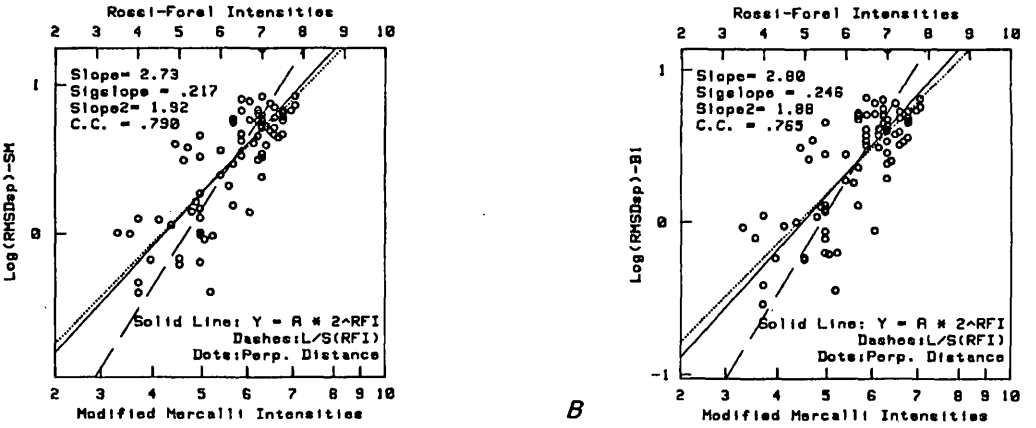

Figure 5. RMS displacement versus intensity data for the 1971 San Fernando earthquake. *A*, Full bandwidth. *B*, Band 1 (0.1–0.5 Hz). Data for all stations except those having Rossi-Forel intensities between 6.8 and 7.2, where decimation is by a factor of 2. Ground condition correction of intensities. Lines and parameters are as described in the text.

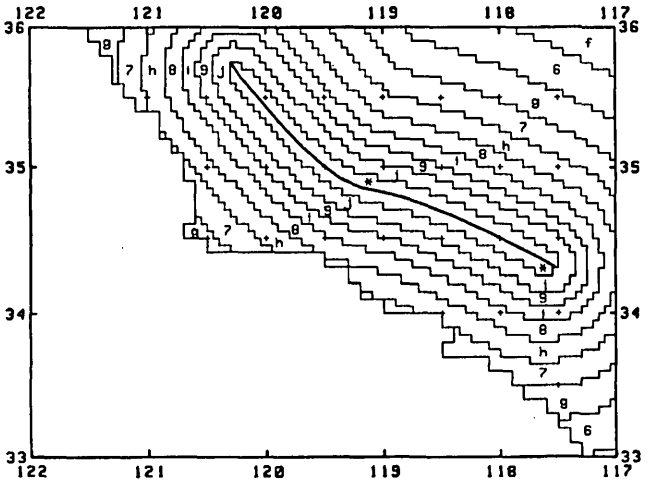

Figure 6. Predicted Rossi-Forel intensities for a repeat of the Fort Tejon earthquake of 1857. Uniform ground condition of saturated alluvium (J). Minimum intensity is V. Arabic numbers indicate the lower half of an intensity value (9 is the lower half of IX), and letters indicate the upper half (j is the upper half of IX). Asterisks indicate the lower half of X.

intensities, and figures 8*B*, 9*B*, and 10*B* give predicted Modified Mercalli intensities (as measured on saturated alluvium) (see table 1) perpendicular to the fault strike for earthquakes of varying length, surface wave magnitude M, and moment Mo in regions where $k=1.75$ (that is, western California). It is apparent immediately that there is remarkable agreement between the data for California earthquakes (the Mammoth Lake earthquake not being used, since its epicenter is deep within the region of $k=1.5$) and the predicted intensities for California earthquakes.

It seems certain that the merging of data from earthquakes of different regions into a composite curve led both Wilson and Keefer (1985) and Youd and Perkins (1978) into a misinterpretation of their data. The data for coherent slides and for lateral spreads and flows (figs. 8*A*, 9*A*) follow very closely the RFI curve for the intensity VII–VIII boundary (MMI VI–VI+⅓) (figs. 8*B*, 9*B*), while the data for disrupted slides and falls in figure 10*A* follow closely the RFI VI–VII boundary beyond M 5.5 (approximately MMI V–VI) (fig. 10*B*). We conclude that, when properly interpreted, the observed data for ground failure phenomena agree very closely with intensity values and are thus predictable on the basis of predicted Rossi-Forel or Modified Mercalli intensities. The pertinent curves for use within our predictive model will be given in Part II of this paper (figs. 13*A*, 13*B*).

As we pointed out above and in our earlier paper (Evernden and Thomson, 1985), intensity values correlate closely with strong motion parameters in the bandpasses from 0.5 to 3 Hz and from 3 to 10 Hz but not with bandpasses from 0.1 to 0.5 Hz and from 10 to 25 Hz. Correlation of ground failure with intensity then implies that ground failure is linked to strong ground motion in part or all of the frequency range from 0.5 to 10 Hz.

Discussion of the apparently highly discordant datum at magnitude 6.4 ($2L=20$ km) in figures 8 and 9 is important, as this datum illustrates clearly the danger in attempting one-parameter interpretation of multiparameter data. These data are for the 1966 Parkfield, Calif., earthquake, an earthquake with a demonstrable break of 20 to 30 km and a surface-wave magnitude M of about 6.4. Why are the data from this event in such marked disagreement with the other California data? Fortunately, there is a clear explanation, supported by unequivocal seismological observations (Lindh and Boore, 1981). By great good luck, short-period seismometers in the immediate vicinity of this earthquake clearly recorded that

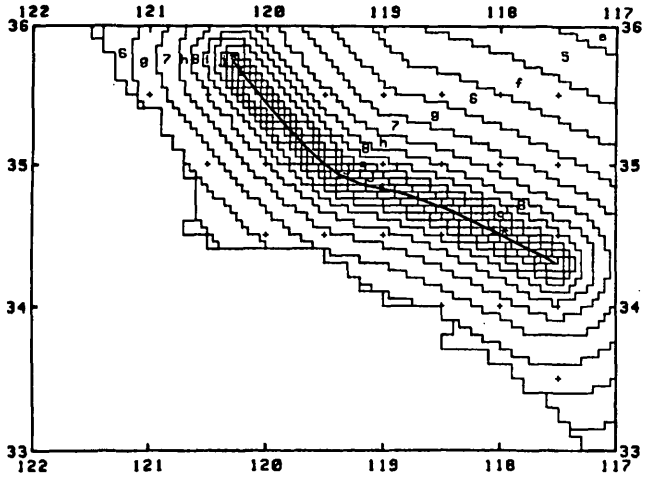

A. 0.5 Hz, 5 percent damping.

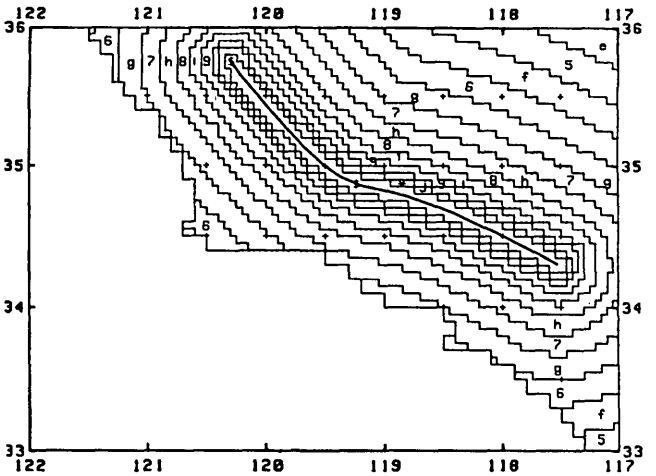

B. 1 Hz, 5 percent damping.

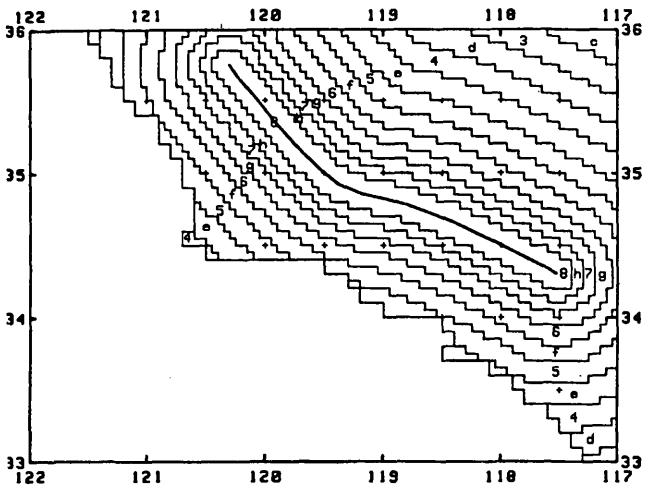

C. 5 Hz, 5 percent damping.

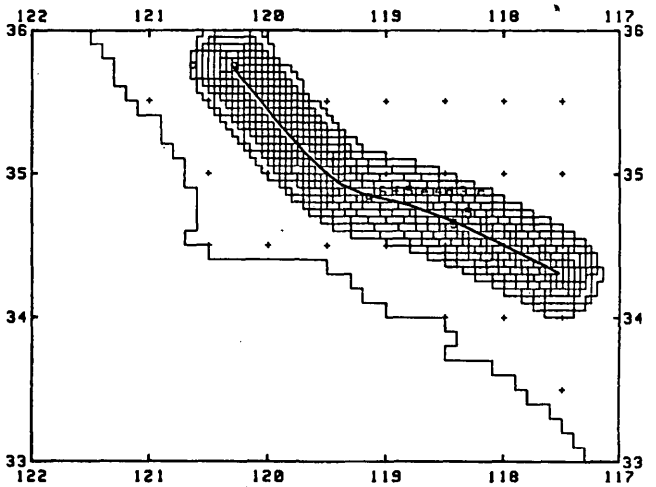

D. 10 Hz, 5 percent damping.

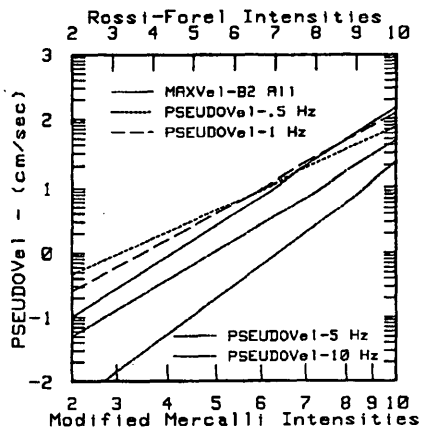

E. Interpreted relationship between intensity and pseudovelocity (5 percent damping).

Figure 7. Predicted pseudovelocity (in centimeters per second) for a repeat of the Fort Tejon earthquake of 1857 (following Joyner and Fumal, 1985). Ground condition is "soil." Arabic numbers indicate the lower half of an intensity value (9 is the lower half of IX), and letters indicate the upper half (j is the upper half of IX). Asterisks indicate the lower half of X.

rupture for this earthquake began to the north and propagated southward with radiation of very low amplitude high-frequency waves for nearly the entire length of the rupture. Only the southerly 3 km of rupture resulted in radiation of "normal" amplitudes of high-frequency waves. Thus, seismic energy at frequencies relevant to ground failure (and other intensity-sensitive parameters) was nearly entirely radiated by the southern 3 km of rupture. As Evernden and others (1981) pointed out, the intensity pattern for this earthquake is consistent with a 3-km rupture at the southern end of the observed rupture,

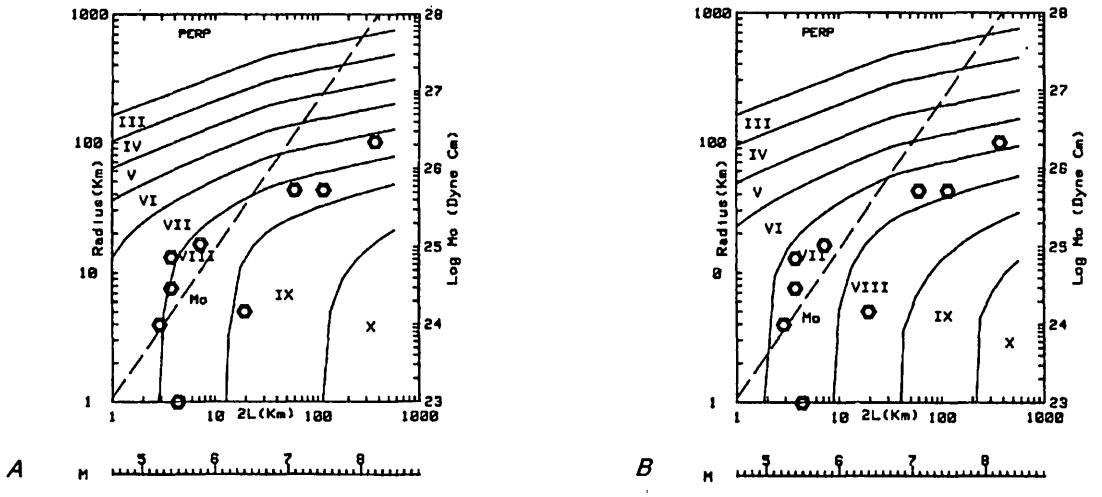

Figure 8. Observed maximum distances (distances from rupture) of coherent slides (pentagons) and (*A*) predicted Rossi-Forel intensities and (*B*) predicted Modified Mercalli intensities versus magnitude and rupture length (2*L*) for earthquakes (solid lines) in western California (k=1.75, C=25). Ground condition is saturated alluvium. See figure 12 for explanation of dashed line Mo. Observations taken from Wilson and Keefer (1985).

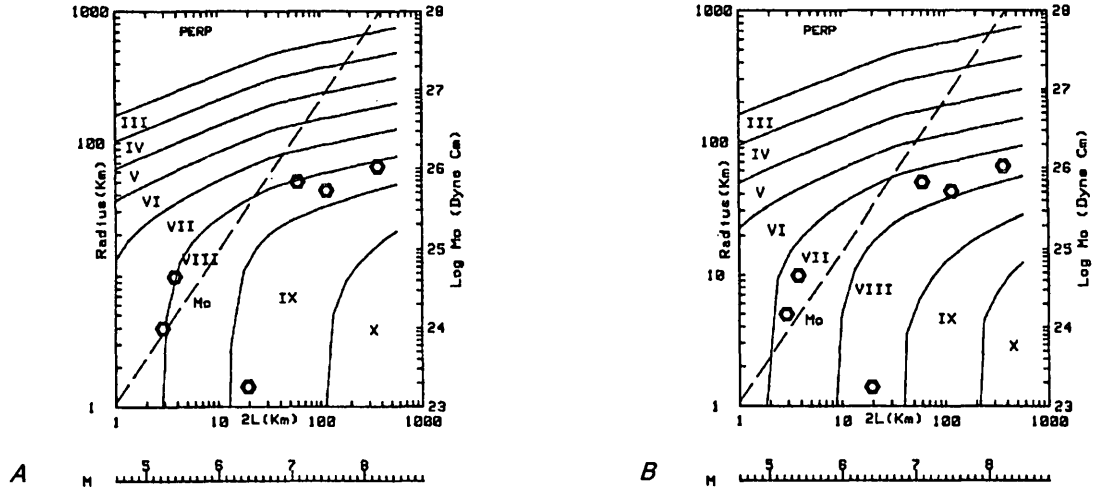

Figure 9. Observed maximum distances (distances from rupture) of lateral spreads and flows (pentagons) and (*A*) predicted Rossi-Forel intensities and (*B*) predicted Modified Mercalli intensities versus magnitude and rupture length (2*L*) for earthquakes (solid lines) in western California (k=1.75, C=25). Ground condition is saturated alluvium. See figure 12 for explanation of dashed line Mo. Observations taken from Wilson and Keefer (1985).

while the surface-wave amplitudes indicate a rupture length of 20 to 30 km. Within the earthquake model described in detail by Evernden and others (1986) and discussed by Evernden and Thomson (1985), the physical explanation for such behavior is slow rupture for the first many kilometers of break and normal rates of rupture ($U_R \simeq V_S$) for only the final 3 km, where U_R is the rupture velocity and V_S is the shear-wave velocity in rocks adjacent to the fault. Since, as noted above, figures 8 through 10 indicate correlation of ground failure with intensity-relevant frequencies (0.5 to 3 or 10 Hz), it is clear that the Parkfield datum on figures 8 and 9 should be moved to a rupture length of 3 km, a position that would show agreement with all of the other California data. It must always be kept in mind that the seismological world is never one dimensional, and efforts to so treat it will often lead to serious misinterpretation.

PART II: MODEL FOR PREDICTING GROUND MOTION AND DAMAGE PARAMETERS OF EARTHQUAKES

Given the correlations of strong motion and ground failure parameters with intensity discussed in Part I, the correlations of structural damage and intensity presented by Evernden and Thomson (1985) and the model given by Evernden and others (1981) for predicting seismic intensities throughout the several different geotectonic regions of the United States (and thus of the world), we are now

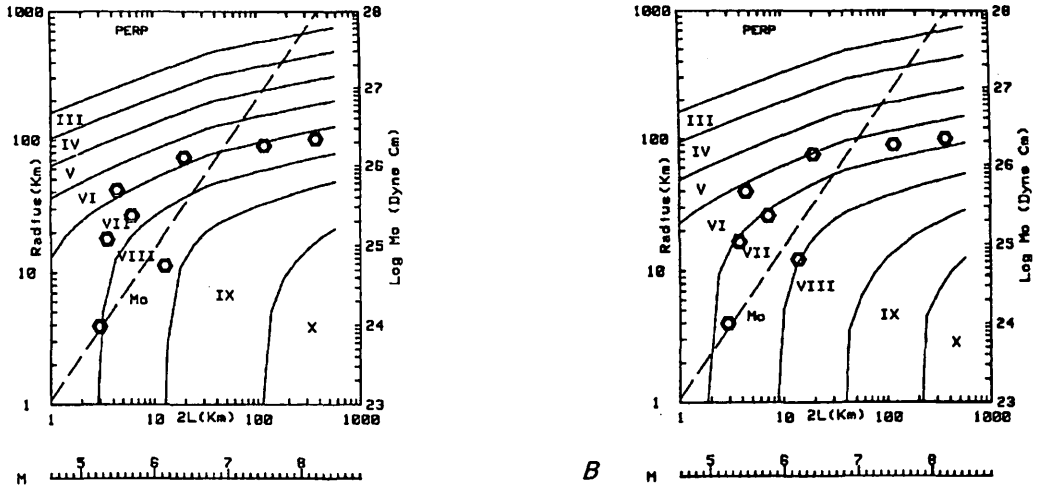

Figure 10. Observed maximum distances (distances from rupture) of disrupted slides or falls (pentagons) and (*A*) predicted Rossi-Forel intensities and (*B*) predicted Modified Mercalli intensities versus magnitude and rupture length (2*L*) for earthquakes (solid lines) in western California (k=1.75, C=25). Ground condition is saturated alluvium. See figure 12 for explanation of dashed line Mo. Observations taken from Wilson and Keefer (1985).

in a position to develop a generally applicable model for predicting all of the above parameters for earthquakes throughout the United States and the world. Detailed confirmation or modification of the model must await testing against observations from regions other than western California.

For application of the model in any specific area, one must have established the appropriate rate of decrease of intensity with distance. This rate can be found either by studying intensity maps for previous earthquakes of the area or by establishing, by using any of several geophysical parameters, the geotectonic equivalence of the area of interest and a region of known attenuation characteristics (Evernden, 1983). Such study finally leads to selection of the appropriate k (or attenuation) value (Evernden and others, 1981; Evernden, 1983). Figure 11 presents the pattern of k values found for the conterminous United States by studying intensity maps of U.S. earthquakes (Evernden and others, 1981), while Evernden (1983) presented a comparable map for eastern Asia.

If the selection of k value is determined by study of local intensity patterns, it will be necessary to establish the correlation of the local intensity scale with MMI or RFI values. Even if the selection of k value is reached by other means, it will still be necessary to establish the correlation of the local intensity scale with RFI or MMI in order to be able to use the following figures, expressed as they are in terms of RFI and MMI. In regions where building types differ markedly in character from those used to define RFI and MMI units, new definitions of those units may need to be established in terms of local structure types, including percentage of damage versus intensity versus structural type. Massive confusion results if intensity is defined in terms of percentage of damage to structures without regard for structural type and (or) quality of construction. This failure to modify definitions of intensity units as structural types are modified (as, say, the earthquake resistance of structures is improved, as it has been in California in recent decades) is already leading to great confusion in interpreting the intensity maps of recent earthquakes.

Finally, it will be necessary to establish the physical equivalence of local geologic units to those used in California in order to be able to use table 1 for adjusting intensities predicted for saturated alluvium to those predicted for other rock types. Table 2, repeated from papers by Evernden and others (1981) and Evernden and Thomson (1985), presents the correlation of the geologic units of the State geologic map of California and our shaking units. The codification of the rock units on the State map follows general rules and thus should be understandable to most geologists.

When these tasks have been completed for the region of interest, the application of the model is straightforward.

Step 1.—Select from figures 12*A*–*J* the one having the k and pseudodepth (C) values appropriate to the earthquake to be modeled

If a U.S. earthquake is being modeled, find the k value by inspection of figure 11. If an earthquake elsewhere is being modeled, establish the geotectonic equivalence of the area of interest and a portion of the United States, and then use figure 11. Evernden (1983) presented a figure that was similar to figure 11 of this paper but that applied to eastern Asia (the People's Republic of China and surrounding areas).

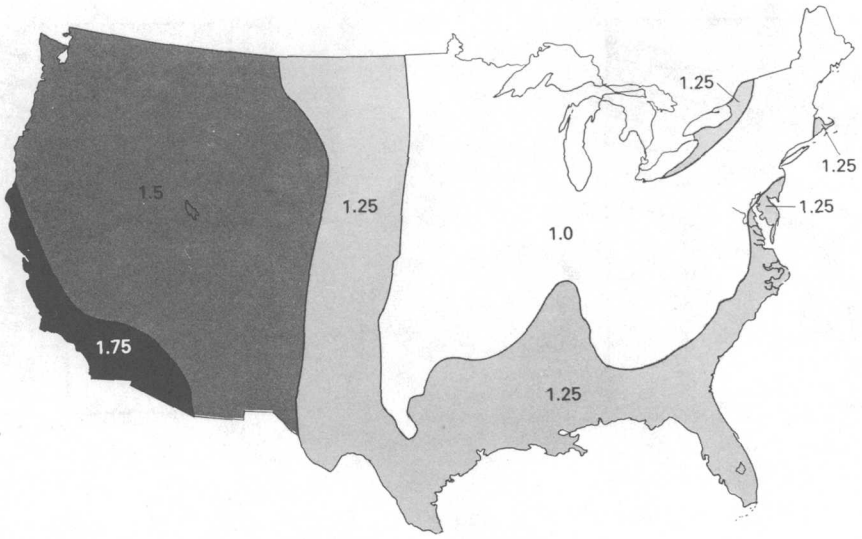

Figure 11. Approximate pattern of *k*-value distribution throughout the conterminous United States.

Figure 11 is divided into areas characterized by k values of 1.75, 1.50, 1.25, and 1.00 (k value increases in increments of 0.25). This set of k values is generally adequate. However, Evernden (1983) found, in his study of Chinese earthquakes, that use of k values at increments of 0.125 was useful. Also, investigation of some California earthquakes (Evernden and others, 1981) suggested that k values such as 1.875 and 1.625 occasionally appeared to achieve marginally better fits to observations than did k=1.75. Therefore, figures having such k values are included.

Figures 12*A* through 12*J* are labeled to facilitate the proper selection for a particular case. A few additional comments may be useful.

In general, it should be adequate to use only the k values of 1.75, 1.50, 1.25, and 1.00. Thus, figures 12*A* and 12*D* are to be used only when specifically indicated or when investigating the influence of a slight change in k value.

The two C values of 25 and 20 for western California earthquakes (figs. 12*B*, 12*C*) are intended for use with strike-slip earthquakes (for example, on the San Andreas fault) and thrust earthquakes (for example, the San Fernando earthquake), respectively.

All significant earthquakes in the Seattle area of Washington (fig. 12*E*, k=1.50) have been at depths of 40 km or greater. Evernden and others (1981) showed that a C value of 60 yielded predicted intensities in agreement with observations for the 1949 Seattle earthquake. Therefore, figure 12*E* is for a C value of 60. The effect of a C value of 25 (focal depth of 10 km or so) would be to predict markedly higher intensities in the epicentral area. Figure 12*F* can be used to consider a shallower earthquake in the Seattle area.

Table 2. Correlation of map units on geologic map of California with relative shaking units

Geologic map units	Relative shaking unit
Granitic and metamorphic rocks (Kjfv, gr, bi, ub, JT, m, mV, PpV, Cv, Dv, pS, pSv, pCc, pCgr, pC, epC, TI)	A
Paleozoic sedimentary rocks (Ms, PP, Pm, C, CP, CM, D, S, pSs, O, E)	B
Early Mesozoic sedimentary rocks (Jk, Ju, JmE, Tr, Kjf)	C
Cretaceous through Eocene sedimentary rocks (Ec, E, Epc, Ep, K, Ku, KE)	D
Undivided Tertiary sedimentary rocks (QTc, Tc, TE, Tm)	E
Oligocene through middle Pliocene sedimentary rocks (PmEc, PmE, Mc, Muc, Mu, Mmc, ME, ϕe, ϕ)	F
"Pliocene-Pleistocene" sedimentary rocks (Qc, OP, Pc, Puc, Pu)	G
Tertiary volcanic rocks (Pv, Mv, Olv, Ev, QTv, Tv)	H
Quaternary volcanic rocks (Qrv, Qpv)	I
Quaternary sedimentary deposits (Qs, QaE, Qsc, Qf, Qb, Qst, QE, Qq, Qt, Qm)	J

Available analysis suggests that focal depths of earthquakes in the Basin and Range area (k=1.50) of the United States are very similar to those of earthquakes in western California. Therefore, figure 12*F* (k=1.50, C=30) is intended for use in these areas. An earthquake having a focal depth of 40 to 50 km could be modeled by using the Seattle figure (fig. 12*E*).

Again, available analysis indicates quite shallow focal depths for earthquakes in the eastern United States, in regions of both k=1.25 and k=1.0. Therefore, figures 12*G* and 12*H* are for k=1.25 and C values of 30 and 40, respectively. Figures 12*I* and 12*J* are for k=1.00 and C values of 30 and 40.

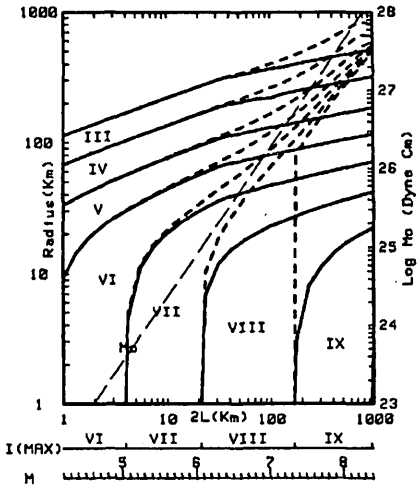

A. Western California earthquakes, where k=1.875 and C=25.

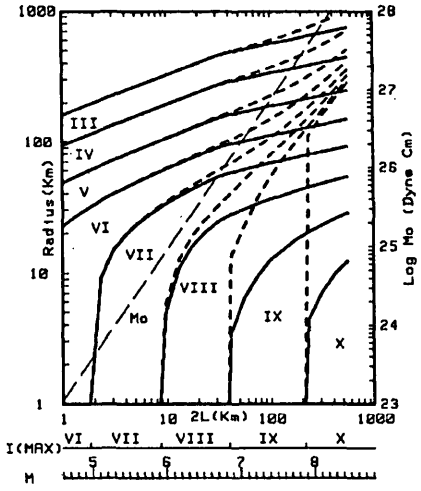

B. San Francisco and Los Angeles earthquakes, where k=1.75 and C=25.

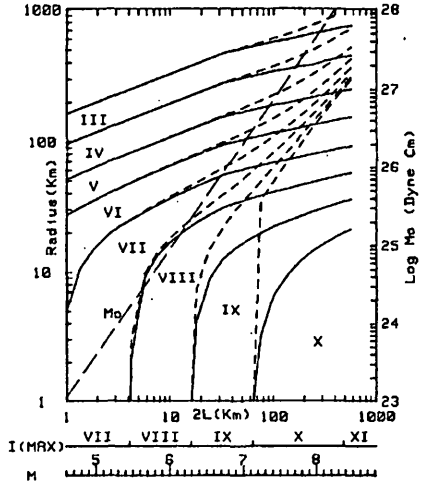

C. Western California earthquakes, where k=1.75 and C=20.

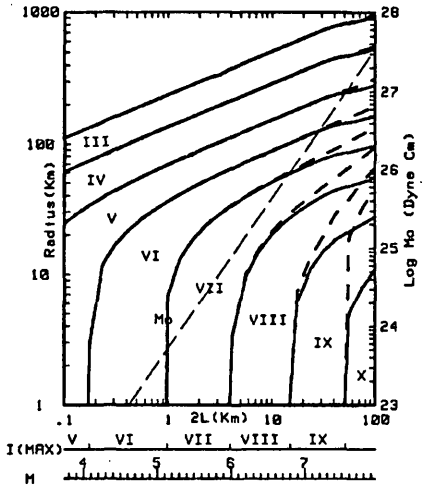

D. Western U.S. earthquakes, where k=1.625 and C=25.

Figure 12. Predicted Modified Mercalli intensity patterns for earthquakes where the ground condition is saturated alluvium. Solid lines are distances perpendicular to the rupture for points between the two ends of the fault. Dashed lines are distances along the strike of the fault from the center of the rupture. $2L$ is the length of rupture, M is the surface wave magnitude M_S, and I(MAX) is the maximum intensity on saturated alluvium. The moment Mo of the earthquake can be found by starting from either M or $2L$, moving vertically to the intersection with the dashed line labeled "Mo," and then moving horizontally to the right and reading Mo.

Figures 12*A* through 12*J* are drawn for Modified Mercalli intensities, as most practitioners use it, even though it is less physically interpretable than the RFI scale is. The predicted intensities in figure 12 are for saturated alluvium.

Step 2.—Decide on length of rupture of earthquake to be modeled

Many would rather decide on the magnitude M (M_S) of the earthquake to be modeled rather than the length of rupture. Figure 12 allows such a selection, but the current confusion in the literature about the correlation of magnitude M_S and length of rupture makes explicit analysis by using length of rupture a better procedure. At the very least, study figure 12 and note the drastic change in the relationship of magnitude versus length of rupture ($2L$) as the k value varies from 1.75 to 1.00. Thus, M=8 is correlated with a $2L$ value of 400 km in regions of k=1.75 and with a $2L$ value of 3 km in regions where k=1.00. This point was elaborately discussed by Evernden and others (1981).

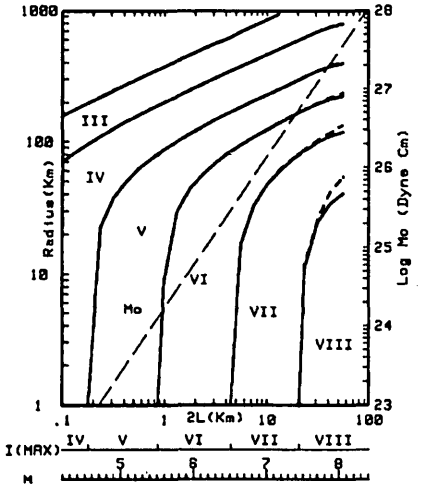

E. Seattle earthquakes, where $k=1.50$ and $C=60$.

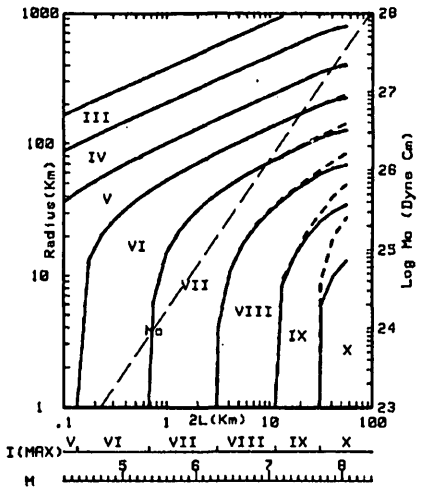

F. Utah and Nevada earthquakes, where $k=1.50$ and $C=30$.

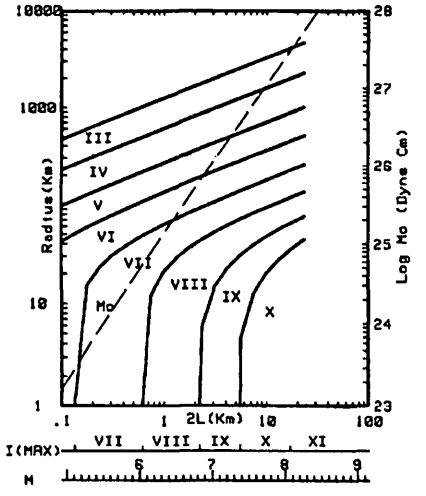

G. Atlantic coast–Mississippi embayment earthquakes, where $k=1.25$ and $C=30$.

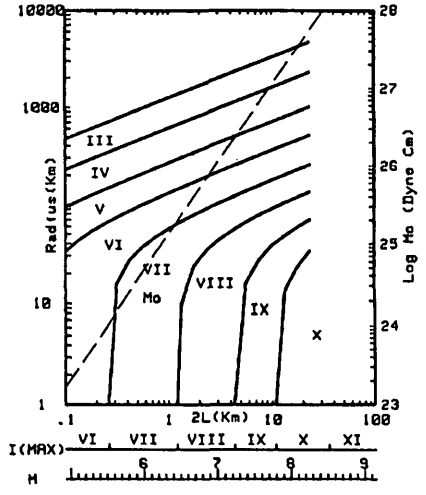

H. Atlantic coast–Mississippi embayment earthquakes, where $k=1.25$ and $C=40$.

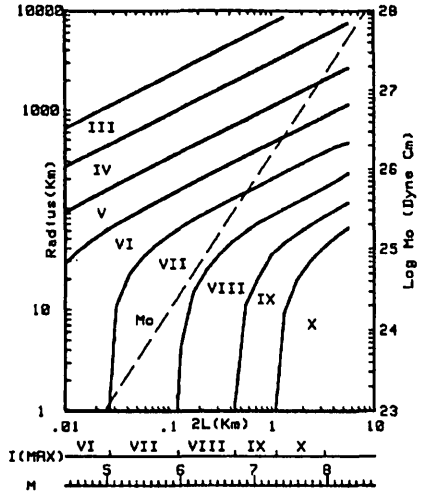

I. Eastern U.S. earthquakes, where $k=1.00$ and $C=30$.

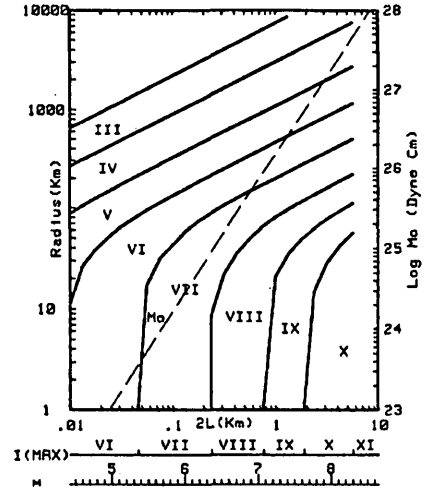

J. Eastern U.S. earthquakes, where $k=1.00$ and $C=40$.

Figure 12. Continued.

Step 3.—Read intensity on saturated alluvium at desired locality

For strike-slip earthquakes, the "desired locality" is defined by rectangular coordinates based on the fault strike, the (0, 0) point of the coordinates being at the center of the modeled rupture. For thrust earthquakes, the center of coordinates should be about 6 km in the downdip direction from the center of the surface rupture. The desired locality can be either a single point, a series of specific localities, or an entire map area.

For regions characterized by k values of 1.25 and less, the intensity contours on uniform ground condition very closely approximate circles centered on the central point of the rupture. Therefore, all points at the same radial distance from the center are predicted to have the same intensity (uniform ground condition). So, determine the distance in kilometers of a desired locality from the center of rupture, find this distance along the vertical axis (labeled "Radius(Km)") of the appropriate figure, and read the predicted Modified Mercalli intensity for the $2L$ value (or M value) appropriate to the modeled earthquake. Thus, in figure 12*J*, for a $2L$ value of 1 km and a radial distance of 200 km, read a predicted MMI value of VI.5 (that is, boundary between MMI VI and MMI VII). Also, read from the lower scales of the figure that such an earthquake would be of about M_S=7¼, the maximum intensity expected on saturated alluvium being MMI IX. If one wishes to draw an intensity map for an earthquake in these k regions, read from the appropriate figure the distance to each of the intensity boundaries and draw circles of these radii centered on the middle of the hypothesized fault rupture.

For k values of 1.5, the intensity contours are no longer circles at short distances for large earthquakes. However, for earthquakes of M_S=7 or less in regions of k=1.50, the predicted intensity contours are so nearly circular that the assumption of circularity is legitimate. In regions where k=1.75 and for earthquakes of M=6.0 or less, the procedures described for k=1.25 or less can be used. In regions where k=1.50 or greater and for larger earthquakes, slightly different procedures must be followed.

For k=1.50 and greater, two types of distances (labeled "Radii") are given on figure 12. One is measured perpendicular to the modeled fault (solid lines), while the other is measured parallel to the modeled fault (dashed lines) along the strike of the fault, distances being measured from the central point of the fault. Strictly, the solid-line distances are perpendicular distances from the center of the fault. However, the intensity contours are so nearly parallel to the fault for the length of the fault that the solid-line distances can be applied to the entire region bounded by lines perpendicular to the fault and passing through the ends of the modeled break.

For regions beyond the fault line, two procedures giving nearly the same answers are possible:

1. Assume that the intensity contours beyond the ends of the fault are semicircles meeting tangentially the intensity contours determined above for the regions along the length of the rupture. For this procedure, measure the distance of a desired locality from the nearest end of the rupture and then use the solid-line distances on the appropriate figure and at the appropriate $2L$ value for determining the predicted intensity on saturated alluvium.
2. Actually, procedure 1 slightly overpredicts intensity, as the intensity contours beyond the fault break are slightly flatter than circles; that is, the distance to a specific intensity value along the strike of the fault is less than the distance to that intensity contour perpendicular to the fault. A minor correction can be made if desired by using the dashed-line curves of the figures, remembering that the dashed-line distances are measured from the center of the rupture (not the end). For nearly all purposes, however, use of semicircular intensity contours in procedure 1 should be adequate.

The product of this step is either predicted Modified Mercalli intensities on saturated alluvium at a set of specified map points or a drawn contour map of predicted Modified Mercalli intensities on saturated alluvium. If one would rather have values in Rossi-Forel intensities, read, from any one of figures 1 through 5, the Rossi-Forel–Modified Mercalli equivalence and generate the desired table of RFI values or the desired RFI map.

From here on, one uses figures presenting the empirically determined correlations of Rossi-Forel and Modified Mercalli intensities with a wide variety of ground effects and damage scenarios. Some of the following steps can be used and some can be ignored in any given study.

Step 4.—Determine distances to various types of ground failure

Figures 13*A* and 13*B* give the predicted correlation of k value, magnitude M_S, and maximum expected distance of the various types of ground failure investigated by Wilson and Keefer (1985). Figure 13*A* is for lateral spreads and flows as well as for coherent slides. The curves are developed by noting the empirical correlation in figures 8*A*, 8*B*, 9*A*, and 9*B* between these ground failure types and intensity of western California earthquakes (k=1.75) and then drawing on figure 13*A* this intensity boundary as predicted in the several regions of different k values. The slightly erratic behavior of the predicted lines at low magnitude is a product of the digitized character of

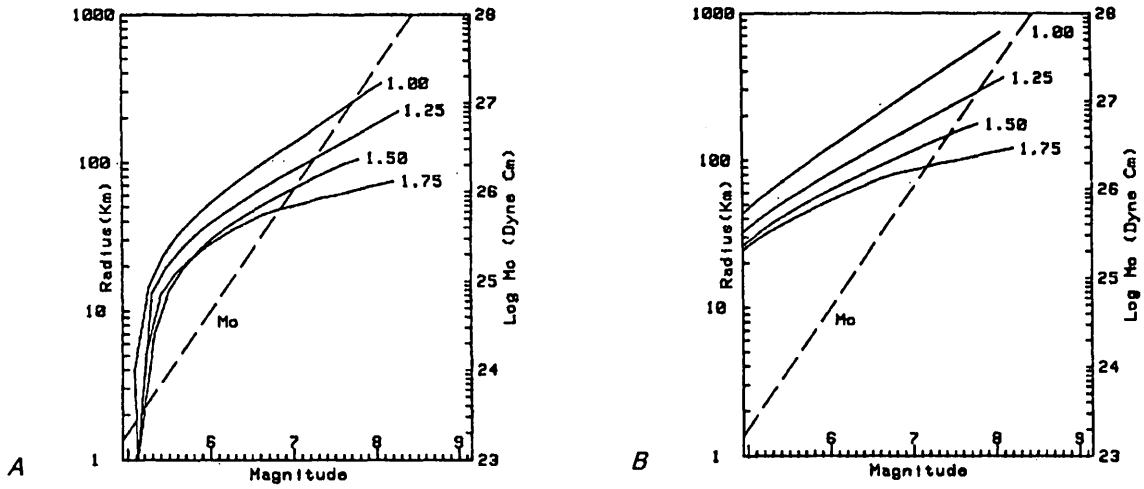

Figure 13. Predicted limit of ground failure for (*A*) lateral spreads, flows, and coherent slides and (*B*) disrupted slides and falls in regions of different k values. Distances are measured perpendicular to the modeled fault, similar to those in figure 12. It should be remembered that occurrence of ground failure requires not only the requisite ground motion at the proper frequencies but also the proper terrain and soil deposits. Regions where $k=1.75$ are characterized by high rates of uplift, steep slopes, and uplifted weak sediments. Regions where $k=1.00$ are characterized by little or no uplift and gentle to flat slopes, and nearly all hills or valley walls are of hard rocks. Thus, this figure may well overpredict the extent of ground failure in regions of low k value, as it is based on the principle of equal probability of ground failure at the same intensity in all k regions.

the calculation procedures and is to be ignored. Figure 13*B*, for disrupted slides, was developed in a similar way and is based on figures 10*A* and 10*B*.

Step 5.—Calculate intensity(ies) for proper ground condition(s)

By using tables 1 and 2 and a table generated by the user correlating the geologic rock units of California with those of the region of interest, calculate the predicted intensities at all desired localities for the actual ground conditions at those sites. All intensity adjustments are negative; that is, all adjusted intensities are less than those predicted for saturated alluvium. In loose alluvium, take account of depth to water table, as table 1 indicates.

Step 6A.—Determine ground motion parameter of interest by using least-squares estimates of correlations with intensity
OR
Step 6B.—Determine ground motion parameter of interest by using slope value of 2 and passing through (Xbar, Ybar)

As we noted in Part I, the least-squares estimates of the linear correlation of Rossi-Forel intensity and strong motion parameter are always slightly to markedly in excess of the slope value of 2 used in the model for predicting intensities. However, the differences for maximum velocity and RMS acceleration in the intensity bandpass (band 2) are so minor as to give clear support to the model. In these cases and in numerous others, it is not obvious that using the least-squares estimate of slope is superior to simply using a slope value of 2. Therefore, two sets of relationships between ground motion parameters and intensity are given; those based on the slope values are determined by least squares (figs. 14*A*–14*G* and similar figures), and those based on a uniform slope value of 2 are determined with the constraint that the curve used must pass through the "center of gravity" of the population (Xbar, Ybar). These curves are given in figures 15*A* through 15*E*.

For most ground motion parameters, there was no clear evidence that the functional relationship between parameter and intensity was a function of ground condition. Therefore, most of the curves in figures 14 and 15 are curves for all rock types.

Figures 14*A* and 15*A* are for maximum acceleration, curves being given for least-squares analysis of data for full bandwidth and for the four partial bandwidths. As can be seen, band 1 (0.1–0.5 Hz) shows very low maximum acceleration values, and bands 2 and 3 (0.5–10 Hz) show the highest narrow-band values; values for the full bandwidth are greater than those for any partial bandwidth, and all four of these curves have nearly identical slope values. The curve for band 4 (10–25 Hz) in figure 14*A* displays a markedly different behavior, indicative of a

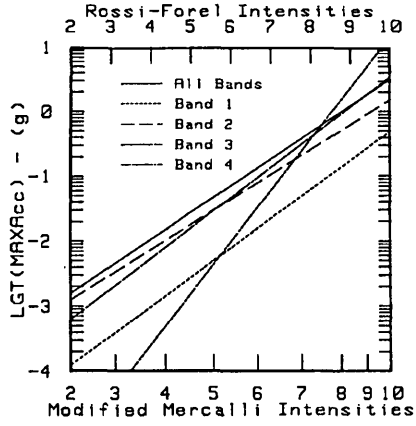

Figure 14*A*. Relationships between Rossi-Forel and Modified Mercalli intensities and maximum acceleration. Data are for all stations (all rock types). Curves are best-fit least-squares curves as described in text, curves for full bandwidth (SM) and bands 1 through 4 being given. Units of acceleration are fractions of *g* (980 Gal).

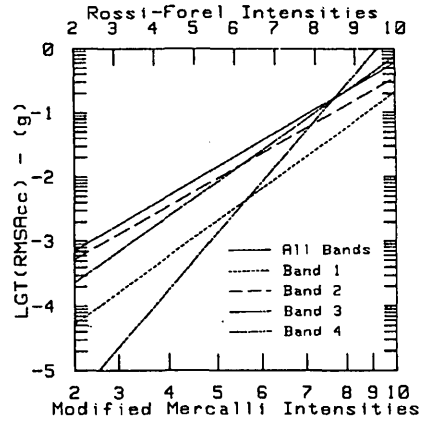

Figure 14*B*. Relationships between Rossi-Forel and Modified Mercalli intensities and RMS acceleration. Data are for all stations (all rock types). Curves are best-fit least-squares curves as described in text, curves for full bandwidth (SM) and bands 1 through 4 being given. Units of acceleration are fractions of *g* (980 Gal). Time window is 10 s for full bandwidth and bands 2 through 4 and 20 s for band 1.

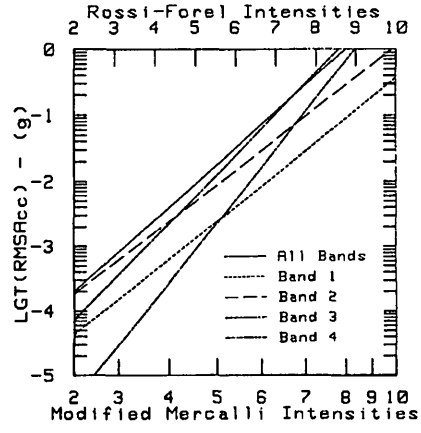

Figure 14*C*. Relationships between Rossi-Forel and Modified Mercalli intensities and RMS acceleration. Data are for stations on alluvium. Curves are best-fit least-squares curves as described in text, curves for full bandwidth (SM) and bands 1 through 4 being given. Units of acceleration are fractions of *g* (980 Gal). Time window is 10 s for full bandwidth and bands 2 through 4 and 20 s for band 1.

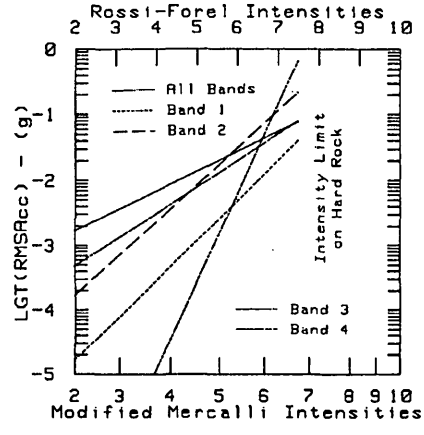

Figure 14*D*. Relationships between Rossi-Forel and Modified Mercalli intensities and RMS acceleration. Data are for stations on hard rock. Curves are best-fit least-squares curves as described in text, curves for full bandwidth (SM) and bands 1 through 4 being given. Units of acceleration are fractions of *g* (980 Gal). Time window is 10 s for full bandwidth and bands 2 through 4 and 20 s for band 1.

very high rate of falloff with intensity and thus with distance.

Figures 14*A* and 15*B* differ from figures 14*A* and 15*A* only in the use of RMS acceleration rather than maximum acceleration. The relationships of the several curves for the various bands are as shown in figures 14*A* and 15*A*. Figures 14*C* and 14*D* are also for RMS acceleration but for subsets of the available data, figure 14*C* being for sites on alluvium and figure 14*D* being for sites on hard rock. The curves for bands 2 and 3 are very similar in both figures, any differences being of questionable statistical significance (see earlier discussion). Band 1 values appear to decrease more rapidly with intensity on hard rock than they do on alluvium. This rapid decrease may simply be because a given intensity on hard rock is at a much shorter epicentral distance, and band 1 values on hard rock are thus able to more clearly display the role of the elastic near-field terms (see earlier discussion). At the same intensity, band 4 values are higher on hard rock (band 2 values being nearly identical), but, at the same range—intensity(alluvium)=intensity(hard rock)+2.5—band 4 values are markedly greater on alluvium.

Figures 14*E* and 15*C* are for maximum velocity versus intensity. Lack of clear evidence for different relationships instigated by rock type resulted in an absence of figures based on differing rock types. The fact that

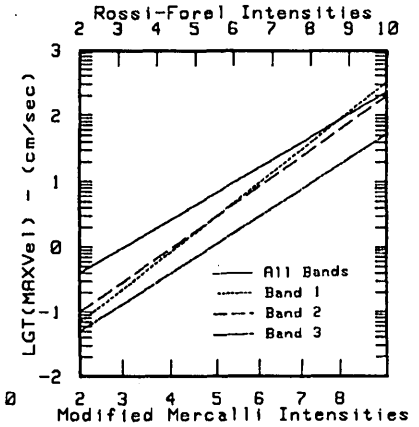

Figure 14*E*. Relationships between Rossi-Forel and Modified Mercalli intensities and maximum velocity. Data are for all stations (all rock types). Curves are best-fit least-squares curves as described in text, curves for full bandwidth (SM) and bands 1 through 3 being given. Units of velocity are centimeters per second.

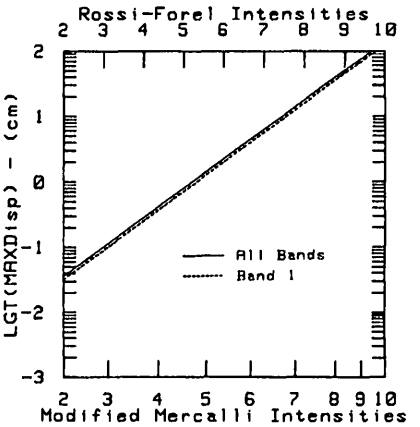

Figure 14*F*. Relationships between Rossi-Forel and Modified Mercalli intensities and maximum displacement. Data are for all stations (all rock types). Curves are best-fit least-squares curves as described in text, curves for full bandwidth (SM) and band 1 being given. Units of displacement are centimeters.

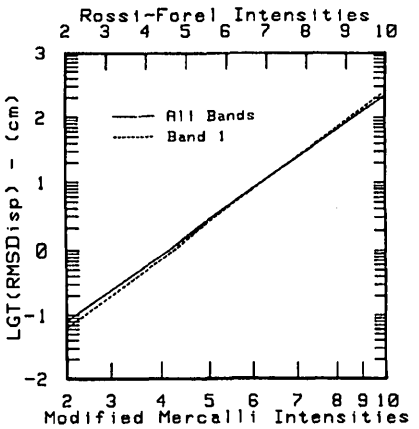

Figure 14*G*. Relationships between Rossi-Forel and Modified Mercalli intensities and RMS displacement. Data are for all stations (all rock types). Curves are best-fit least-squares curves as described in text, curves for full bandwidth (SM) and band 1 being given. Units of displacement are centimeters.

values for band 3 are an order of magnitude below those based on full bandwidth (and bands 1 and 2 at high intensity) made it irrelevant to include band 4 data on the figure.

Figures 14*F* and 15*D* are for maximum displacement, while figures 14*G* and 15*E* are for RMS displacement. The identity of the curves for full bandwidth and band 1 make it irrelevant to include curves for higher frequency bands. Note that maximum displacement at very high intensity is 200 to 300 cm, while RMS displacement (over a 20-s time window) is predicted to be 100 to 200 cm.

For reasons stated by Evernden and Thomson (1985), we strongly recommend using figure 14 rather than figure 15.

Step 7.—Calculate expected value of pseudovelocity versus frequency

Figure 16 (a repeat of fig. 7*E*) presents the correlations of intensity and pseudovelocity (5 percent damping) as a function of frequency found by the investigation described in Part I. As for other parameters, correlation of this figure with predicted values of intensity (either RFI or MMI) can lead to predicted values of pseudovelocity at particular sites and ground conditions or to maps of pseudovelocity as a function of position around the modeled fault rupture. As we pointed out earlier, there was no detectable influence of rock type on the maximum velocity versus intensity relationships found in the study of the strong motion data of the 1971 San Fernando earthquake. Therefore, figure 16 is presumed applicable as a function of intensity independent of rock type.

Step 8.—Derive estimates of expected level of damage to buildings of various types

Figure 17 is a redrafted version of a figure given by Evernden and Thomson (1985), the empirical bases for the curves of this figure being given in the same reference. The curves predict, on the basis of empirical studies, the expected level of damage to buildings of four distinctly different types:

1. Pre-1940 wood-frame construction in California.
2. Post-1940 wood-frame construction in California.

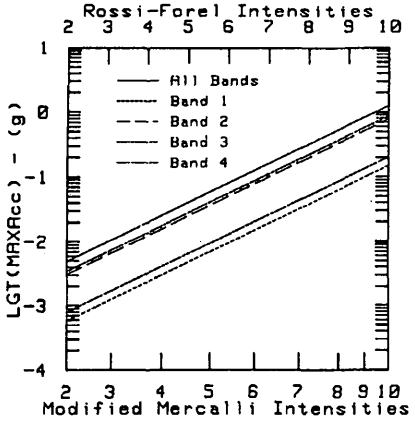

Figure 15*A*. Relationships between Rossi-Forel and Modified Mercalli intensities and maximum acceleration. Data are for all stations (all rock types). Curves have a slope of 2 and pass through Xbar, Ybar, as described in the text, curves for full bandwidth (SM) and bands 1 through 4 being given. Units of acceleration are fractions of *g* (980 Gal).

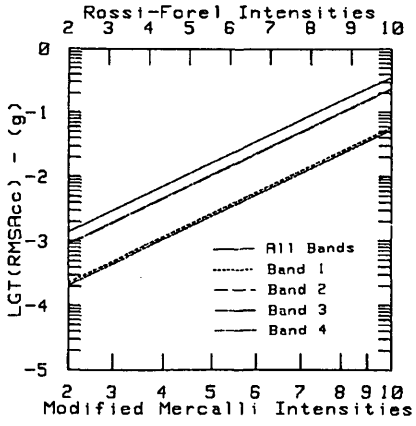

Figure 15*B*. Relationships between Rossi-Forel and Modified Mercalli intensities and RMS acceleration. Data are for all stations (all rock types). Curves have a slope of 2 and pass through Xbar, Ybar, as described in the text, curves for full bandwidth (SM) and bands 1 through 4 being given. Units of acceleration are fractions of *g* (980 Gal). Time window is 10 s for full bandwidth and bands 2 through 4 and 20 s for band 1.

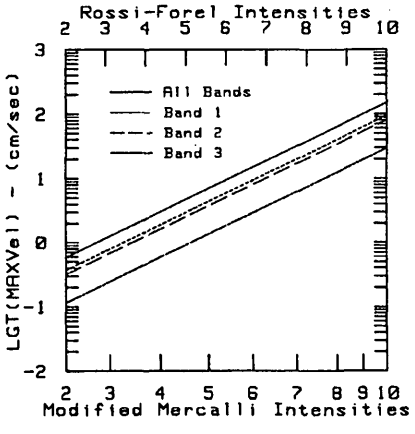

Figure 15*C*. Relationships between Rossi-Forel and Modified Mercalli intensities and maximum velocity. Data are for all stations (all rock types). Curves have a slope of 2 and pass through Xbar, Ybar, as described in the text, curves for full bandwidth (SM) and bands 1 through 3 being given. Units of velocity are centimeters per second.

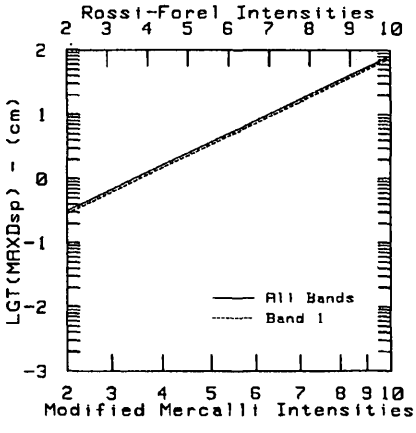

Figure 15*D*. Relationships between Rossi-Forel and Modified Mercalli intensities and maximum displacement. Data are for all stations (all rock types). Curves have a slope of 2 and pass through Xbar, Ybar, as described in the text, curves for full bandwidth (SM) and band 1 being given. Units of displacement are centimeters.

This curve differs from the previous one in assuming the same level of damage at a greater intensity level (VIII.8 instead of VIII.0). As Evernden and Thomson (1985) discussed, this estimate of the protection achieved by the post-1940 code is probably too low.

3. Commercial unreinforced concrete construction.
4. Residential unreinforced concrete construction.

FINAL REMARKS

All of the above relationships (steps 3–8) can be programmed for ease of analysis for a large set of localities or for generation of maps. Many of these relationships have already been so programmed, and the programs are available on request. Figure 18, which is complementary to figure 6, gives predicted values of MMI for a repeat of the Fort Tejon earthquake of 1857, for which figure 6 gave RFI values. For those unfamiliar with the differences between these two scales, a study of figures 6 and 18 may be informative. Also, either of these maps can be converted to maps for other ground conditions by changing intensity units according to the unit designations in tables 1 and 2 and the RFI-MMI scalings indicated on figures 19*A* and 19*B* or similar figures, the

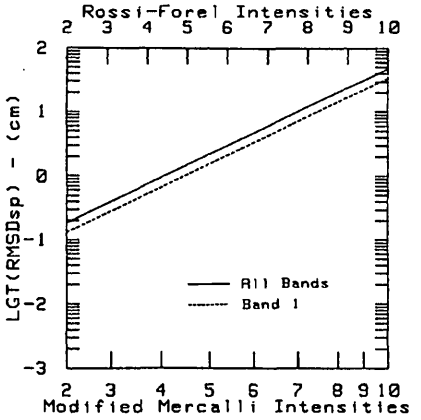

Figure 15*E*. Relationships between Rossi-Forel and Modified Mercalli intensities and RMS displacement. Data are for all stations (all rock types). Curves have a slope of 2 and pass through Xbar, Ybar, as described in the text, curves for full bandwidth (SM) and band 1 being given. Units of displacement are centimeters.

unit designations given in table 1 being in terms of Rossi-Forel intensities.

A few such maps are now presented to illustrate a point of particular significance—the predicted levels of damages to California homes as the result of unavoidable large to great earthquakes in the future. We will not repeat the discussion given by Evernden and Thomson (1985). We will limit ourselves to presentation of maps illustrating the levels of damage predicted by the procedures described above. Figures 19*A* through 20*C* illustrate maps based on data of previous figures. Figures 19*A* and 19*B* indicate along their right-hand margins the definitions of acceleration (fig. 19*A*) and velocity (fig. 19*B*) units used on figures 19*C* through 19*E*. The unit definitions involve a twofold change in the parameter

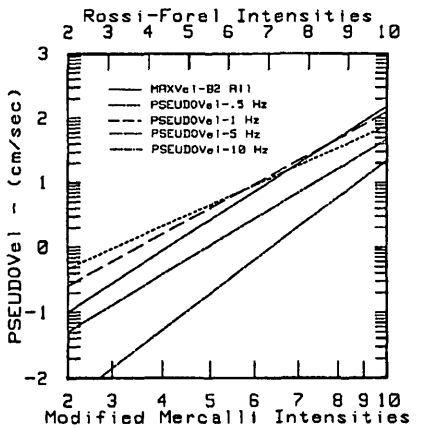

Figure 16. Interpreted relationship between intensity and pseudovelocity (5 percent damping). Ground condition is "soil" (Joyner and Fumal, 1985). See figure 7*E* and associated text.

value for a change of one in the map unit. It seemed irrelevant to define map units for acceleration and velocity values below 0.001 *g* and 1 cm/s, respectively. Each of the following three maps contains the mathematical equation expressing the unit relationships shown in figure 19*A* or 19*B*.

Figure 19*C* presents predicted values of maximum acceleration (full bandwidth) on material of ground condition L resulting from a repeat of the Fort Tejon earthquake of 1857. The values of acceleration and velocity for units 1 through 3 are so low that this figure and the following two figures indicate only unit values of four or greater (0.008–0.016 *g* and 8–16 cm/s). The asterisk and the dollar sign are to be understood as units 10 and 11, respectively. Figure 19*C* indicates a maximum predicted value of maximum acceleration slightly greater than *g* (actually, 1.18 *g* at RFI 8.8 on fig. 19*A* or low RFI IX). Figure 19*A* indicates predicted full bandwidth RMS acceleration under the same conditions to be 0.25 *g*.

Figure 19*D*, for RMS acceleration in band 2 (0.5–3 Hz), indicates maximum predicted values of 0.028 to 0.256 *g* for ground condition L or 0.512 to 0.024 on saturated alluvium or J ground condition (RFI 9.8, fig. 19*A*).

Figure 19*E*, for predicted maximum velocities (full bandwidth) resulting from a repeat of the Fort Tejon earthquake of 1857, indicates maximum velocity values of 64 to 128 cm/s on ground condition L (RFI 8.8). From figure 19*B*, one obtains a predicted maximum velocity on saturated alluvium (RFI 9.8) of 128 to 259 cm/s (unit 9) and on hard rock (RFI 7.3) of 64 to 128 cm/s (unit 7).

Figures 20*A*, 20*B*, and 20*C* illustrate levels of damage to wood-frame structures predicted by our pro-

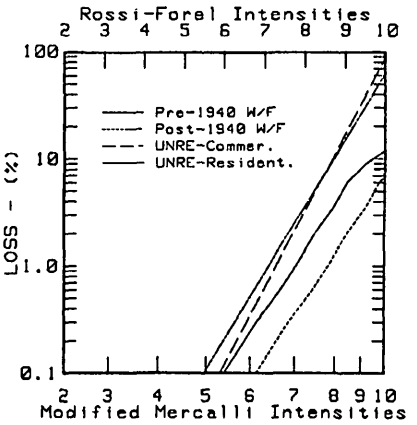

Figure 17. Rossi-Forel and Modified Mercalli intensities versus mean percentage of loss to buildings of various types, all structural types being referenced against construction practice in California. Data sources as noted by Evernden and Thomson (1985). Pre-1940 W/F, pre-1940 wood frame; post-1940 W/F, post-1940 wood frame; UNRE-Commer., commercial unreinforced concrete; UNRE-Resident., residential unreinforced concrete.

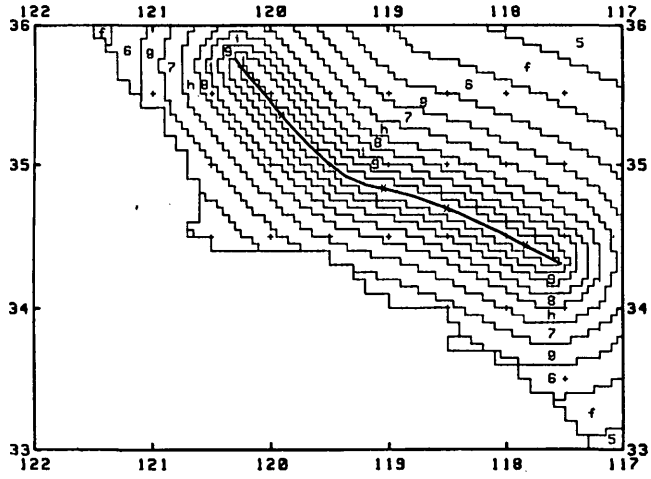

Figure 18. Predicted Modified Mercalli intensities for a repeat of the Fort Tejon earthquake of 1857. Uniform ground condition of saturated alluvium (J). Minimum intensity is V. Arabic numerals indicate the lower half of an intensity value (9 is the lower half of IX), and letters indicate the upper half (j is the upper half of IX). Asterisks indicate the lower half of X. Compare with figure 6 to note differences between the Rossi-Forel and the Modified Mercalli intensity scales.

grams, the reference earthquake again being a repeat of the Fort Tejon earthquake of 1857. Since nearly all Californians live in wood-frame structures meeting the requirements of the post-1940 State building code, investigation of the probable damage to be experienced by such structures is pertinent. A repeat of the Fort Tejon earthquake will, according to some authorities, place many of these structures in southern California at severe risk. Figure 20*A* is the predicted percentage of loss to pre-1940 wood-frame structures on saturated weak alluvium, a building type and a ground condition relevant today to only a few sites in southern California. Reference to the detailed ground condition maps for southern California given by Evernden and Thomson (1985) will illustrate this point. Thus, the 10+ percent loss shown bracketing the entire trace of the proposed rupture along the San Andreas fault is not expressive of reality, as the ground along this portion of the San Andreas is much firmer than that assumed for this map. Even on saturated alluvium, the predicted levels of damage in the greater Los Angeles area constitute a very low percentage of value. The major flaw in pre-1940 wood-frame construction in California was failure to fasten the buildings to a reinforced concrete perimeter foundation. This requirement is part of the post-1940 code. Assuming the relationship shown in figure 17 between percentage of loss and intensity, figure 20*B* presents the predicted level of damage to post-1940 wood-frame structures on saturated alluvium as a result of a Fort Tejon repeat. Note the marked reduction in predicted damage levels, which become inconsequential throughout most of the Los Angeles area. Now, if post-1940 construction is combined with the fact that nearly all structures in southern California are on ground of markedly better quality than saturated alluvium, we can generate a prediction such as that in figure 20*C*. This figure assumes post-1940 construction and a ground condition with an adjustment factor relative to saturated alluvium of −1 (firmer ground or water table at least 10 m below surface of loose alluvium). Note that maximum predicted percentages of loss are now only 2 along the fault rupture and that they are less than 1 to zero throughout essentially all of the built-up areas of southern California. We conclude that estimates of massive damage to residences and the associated vast disruption described by some as a result of this coming earthquake are in gross error. It may be useful to remember that the lives of San Franciscans would have been essentially undisturbed by the earthquake of 1906 if the only problem had been the shaking and associated damage. The disruption in that city was caused by the fire, the shaking having done remarkably little damage to the city. No significant structure experienced 5 percent structural damage; most suffered little or none (Freeman, 1932). We do not mean to imply that repeats of these past earthquakes will not be traumatic events or that there will not be severe problems of several sorts. We do believe, however, that expected levels of damage are being overestimated, to the detriment of proper emergency planning.

A subject requiring careful consideration by users and interpreters of intensity units is the current looseness in use of the Modified Mercalli intensity scale. All definitions of the Rossi-Forel and Modified Mercalli intensity units that incorporate structural damage due to shaking as part of the definition are based on structural styles current in the United States and a few European countries in the first quarter of this century or earlier. They are not based on current construction practice in California, and they never were directly usable in many countries of the world because of complete inconsistency between the structural styles assumed in the definitions and those actually followed in many countries. As Evernden and Thomson (1985) noted, continued application of old definitions of MMI units to communities built under codes far more restrictive than those assumed in the definitions is leading to publication of uninterpretable intensity maps and to consequent confusion (see Evernden and Thomson's (1985) discussion of the Coyote Lake and Imperial Valley earthquakes of 1979). In addition, using these old definitions to estimate expected levels of damage to modern California cities is leading to excessive estimates. Unless more care is taken, the entire science of damage estimation and ground motion estimation will be confused beyond resolution.

There are, of course, obvious ways to solve this developing problem of analysis and interpretation. If

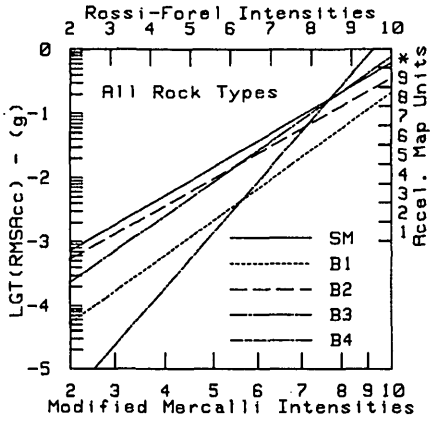

Figure 19*A*. RMS acceleration (all bands) versus intensity and acceleration units (right-hand scale) used on figures 19*C* and 19*D*. The acceleration units apply to either maximum or RMS acceleration.

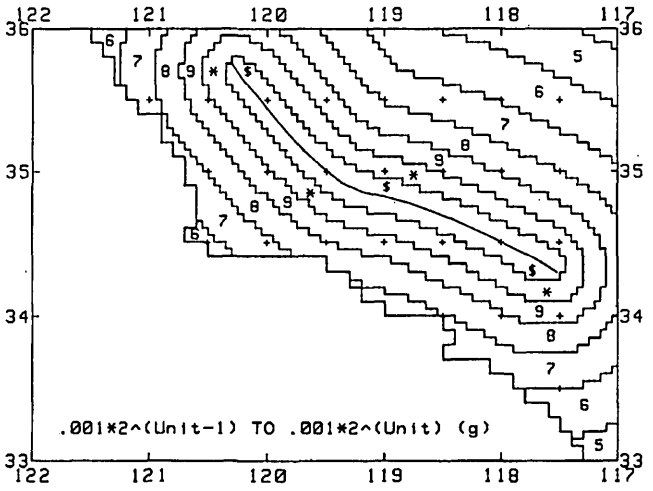

Figure 19*C*. Predicted values of maximum acceleration (full bandwidth) on ground condition L for a repeat of the Fort Tejon earthquake of 1857. Map units are defined on the figure and indicated on figure 19*A*. The asterisk and the dollar sign indicate units 10 and 11, respectively.

interested practioners resolve to promulgate a solution, the developing confusion can be arrested and eliminated. Group inertia much more than unavailability of a solution is the major factor preventing adoption of a generally accepted solution.

We will suggest two somewhat different routes to a definitive and permanent solution. Both depart from the premise that the original definitions must remain valid when applied to the structural types assumed in the original definitions. The two procedures can be briefly described as follows:

1. Greatly expand the current definitions to incorporate damage estimates to the full spectrum of (1) important building types and (2) characteristics that

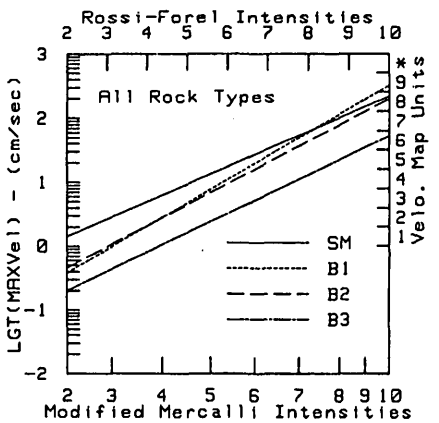

Figure 19*B*. Maximum velocity (all bands) versus intensity and velocity units (right-hand scale) used in figure 19*E*.

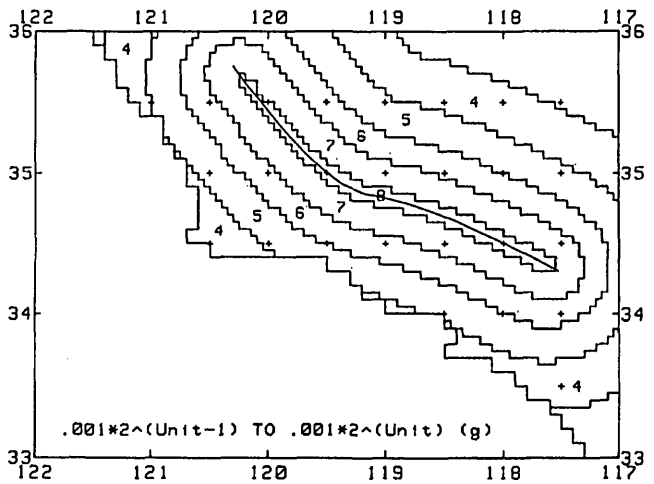

Figure 19*D*. Predicted values of RMS acceleration (band 2, 0.5–3 Hz) for all rock types on ground condition L from a repeat of the Fort Tejon earthquake of 1857. Map units are defined in the figure and indicated in figure 19*A*.

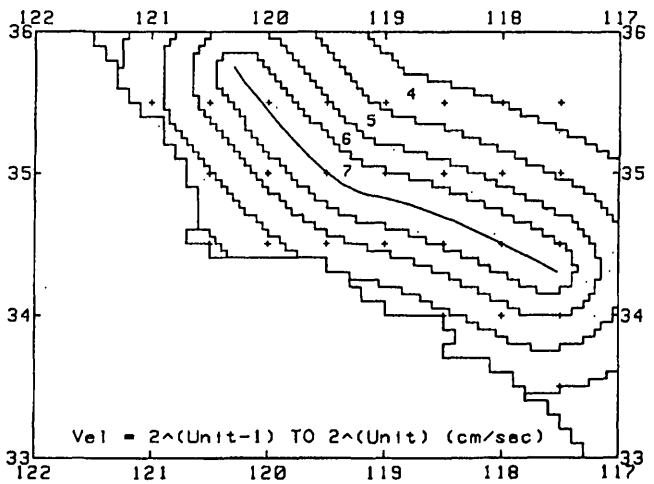

Figure 19*E*. Predicted values of maximum velocity (full bandwidth) on ground condition L for a repeat of the Fort Tejon earthquake of 1857. Map units are defined in the figure and indicated in figure 19*B*.

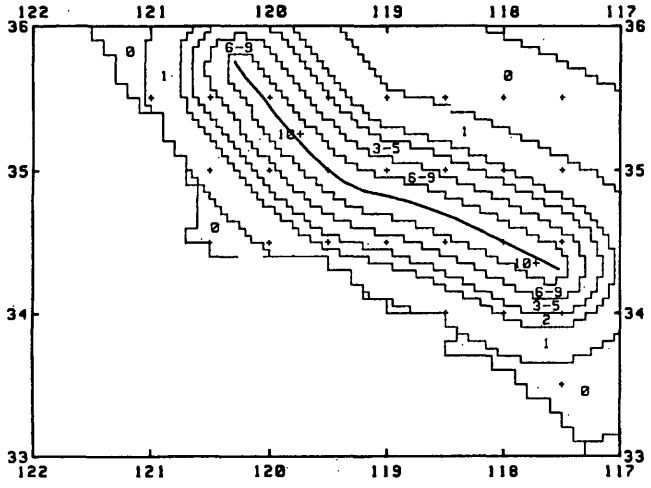

A. Pre-1940 wood-frame buildings on ground condition J.

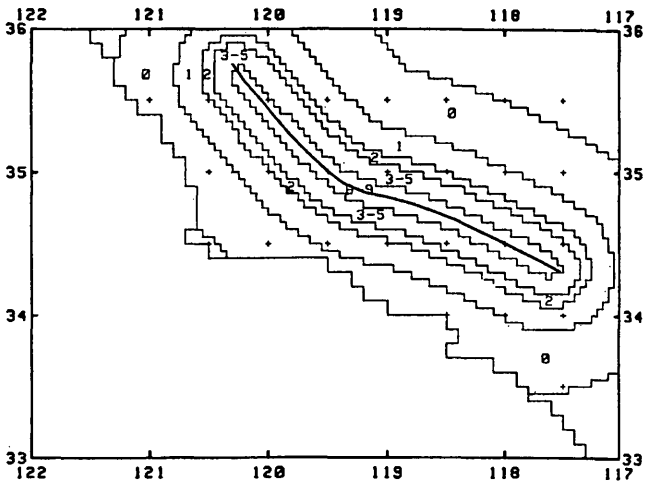

B. Post-1940 wood-frame buildings on ground condition J.

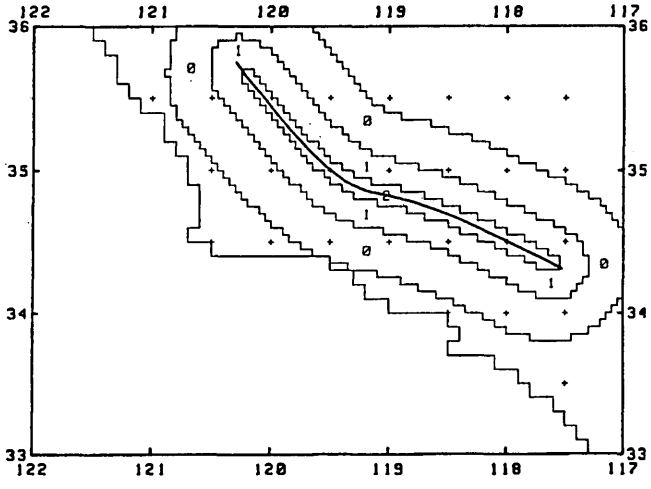

C. Post-1940 wood-frame buildings on ground condition L (one Rossi-Forel intensity unit less than saturated alluvium).

Figure 20. Predicted percentages of loss as a result of a repeat of the Fort Tejon earthquake of 1857. Loss versus intensity relationship is as given by Freeman (1933) and as used by the Association of Bay Area Governments and by others (see Evernden and Thomson, 1985).

respond to energy in the frequency band relevant to the original definitions. This procedure was followed explicitly in the People's Republic of China (Evernden, 1983).

2. Redefine intensity units in terms of expected RMS acceleration (or some other ground motion parameter) in the intensity-relevant bandpass, basing the correlations of ground motion and intensity on the original definitions of the intensity units. Then use tables or figures to express the correlation of expected levels or types of damage to various structural styles.

Although these two procedures appear different formalistically, they are simply different ways of looking at the same solution. Thus, the model given in Part II of this paper can be considered effectively a mix of the two procedures given above. All of the suggested procedures clearly and explicitly address the fundamental problem of the inadequacy of current definitions of intensity units for all current structural types.

It would seem obvious that the most logical procedure would be that described above as procedure 1. One must understand clearly, though, that such definitions would include as elements of intensity IX:

- Total destruction of cities built as Tungshan, China, was before the earthquake that flattened it in 1976.
- Average damage levels to unreinforced concrete structures approaching effectively total loss, although many would not actually collapse.
- Total loss of "modern" buildings that flaunted the reality of earthquake shaking or circumvented the spirit if not the letter of current building codes.
- Only slight damage (none of structural significance) to properly designed wood-frame or reinforced concrete buildings or other properly engineered structures.

Actually, such expanded definitions of intensity units might be useful, as they would effectively state that structural design can indeed defeat the levels of shaking associated with even the largest earthquakes. The problem with this procedure would be the cumbersome character of the requisite definitions. To construct intensity maps of future earthquakes in California, definitions such as those envisaged here will be absolutely necessary if the intensity maps of those earthquakes are to be interpretable relative to maps of older earthquakes.

A final topic for discussion is the need for specific statements within intensity scales of the bandwidth of significance. It is clear from figures given earlier that the data for bands 2 and 3 (0.5–10 Hz) appear to scale similarly relative to current definitions of intensity and to obey nearly the relationship between ground motion and intensity assumed in the predictive model. This bandwidth may require further refinement, but it is quite certain that current intensity definitions link very closely on a physical basis with strong ground motion parameters from 1 Hz to several Hertz. However, it is just as clear that this correlation does not extend to lower and higher frequencies. Thus, ultimately, it would seem desirable to explicitly define frequency-dependent intensity scales. We would suggest that one of the bases of such definitions would be a twofold change in the strong motion parameter for a one-unit change in the frequency-dependent intensity. In this way, all "intensity IX" designations would have the same level of expected ground motion, a probably useful relationship. Since we are not at all sure that the community is yet prepared for such a leap in concept, we forego the pleasure of demonstrating a set of such maps.

REFERENCES CITED

Evernden, J.F., 1975, Seismic intensities, "size" of earthquakes, and related phenomena: Seismological Society of America Bulletin, v. 65, p. 1287–1315.

———1983, Intensity patterns in eastern Asia: Chinese Geophysics, v. 2, p. 405–438.

Evernden, J.F., and Thomson, J.M., 1985, Predicting seismic intensities, *in* Ziony, J.I., ed., Evaluating earthquake hazards in the Los Angeles region—An earth-science perspective: U.S. Geological Survey Professional Paper 1360, p. 151–202.

Evernden, J.F., Kohler, W.M., and Clow, G.D., 1981, Seismic intensities of conterminous United States—Their prediction and interpretation: U.S. Geological Survey Professional Paper 1223, 56 p.

Evernden, J.F., Archambeau, C.B., and Cranswick, E., 1986, An evaluation of seismic decoupling and underground nuclear test monitoring using high frequency seismic data: Reviews of Geophysics, v. 34, p. 143–215.

Freeman, J.R., 1932, Earthquake damage and earthquake insurance: New York, McGraw-Hill, 904 p.

Helley, E.J., Lajoie, K.R., Spangle, W.E., and Blair, M.L., 1979, Flatland deposits of the San Francisco Bay region, California—Their geology and engineering properties, and their importance to comprehensive planning: U.S. Geological Survey Professional Paper 943, 88 p.

Joyner, W.B., and Fumal, T.E., 1985, Predictive mapping of earthquake ground motion, *in* Ziony, J.I., ed., Evaluating earthquake hazards in the Los Angeles region—An earth-science perspective: U.S. Geological Survey Professional Paper 1360, p. 203–220.

Lindh, A.G., and Boore, D.M., 1981, Control of rupture by fault geometry during the 1966 Parkfield earthquake: Seismological Society of America Bulletin, v. 71, p. 95–116.

Tinsley, J.C., and Fumal, T.E., 1985, Mapping Quaternary sedimentary deposits for areal variations in shaking response, *in* Ziony, J.I., ed., Evaluating earthquake hazards in the Los Angeles region—An earth-science perspective: U.S. Geological Survey Professional Paper 1360, p. 127–150.

Wilson, R.C., and Keefer, D.K., 1985, Predicting areal limits of earthquake-induced landsliding, *in* Ziony, J.I., ed., Evaluating earthquake hazards in the Los Angeles region—An earth-science perspective: U.S. Geological Survey Professional Paper 1360, p. 317–346.

Youd, T.L., and Perkins, D.M., 1978, Mapping liquefaction-induced ground failure potential: Proceedings of the American Society of Civil Engineers, Journal of the Geotechnical Engineering Division, v. 104, no. GT4, p. 433–446.

Ziony, J.I., ed., Evaluating earthquake hazards in the Los Angeles region—An earth-science perspective: U.S. Geological Survey Professional Paper 1360, 505 p., 235 figs.